

OPEN ACCESS

EDITED BY

Mariusz Gusiatin, University of Warmia and Mazury in Olsztyn,

REVIEWED BY

Bayram Yuksel, Giresun University, Türkiye Vikas Pandey, Council of Scientific and Industrial Research (CSIR), India

*CORRESPONDENCE

El Saeed R. Lasheen,

□ elsaeedlasheen@azhar.edu.eg

Mabrouk Sami,

⊠ mabrouksami@uaeu.ac.ae

RECEIVED 16 July 2025 ACCEPTED 01 October 2025 PUBLISHED 30 October 2025

CITATION

Saleh GM, Semary HE, Lasheen ESR, Kamar MS, Elkelish A, Sami M, Sanislav IV and Abdelaal A (2025) Metal contamination and radiological risk assessment in the coastal zone of Wadi Ghadir outlet, Red Sea, Egypt. Front. Environ. Sci. 13:1667069. doi: 10.3389/fenvs.2025.1667069

COPYRIGHT

© 2025 Saleh, Semary, Lasheen, Kamar, Elkelish, Sami, Sanislav and Abdelaal. This is an openaccess article distributed under the terms of the Creative Commons Attribution License (CC BY). The use, distribution or reproduction in other forums is permitted, provided the original author(s) and the copyright owner(s) are credited and that the original publication in this journal is cited, in accordance with accepted academic practice. No use, distribution or reproduction is permitted which does not comply with these terms.

Metal contamination and radiological risk assessment in the coastal zone of Wadi Ghadir outlet, Red Sea, Egypt

Gehad M. Saleh¹, Hatem E. Semary², El Saeed R. Lasheen^{3*}, Mohamed S. Kamar¹, Amr Elkelish⁴, Mabrouk Sami^{5*}, Ioan V. Sanislav⁶ and Ahmed Abdelaal⁷

¹Nuclear Materials Authority, Cairo, Egypt, ²Department of Mathematics and Statistics, College of Science, Imam Mohammad Ibn Saud Islamic University (IMSIU), Riyadh, Saudi Arabia, ³Geology Department, Faculty of Science, Al-Azhar University, Cairo, Egypt, ⁴Biology Department, College of Science, Imam Mohammad ibn Saud Islamic University (IMSIU), Riyadh, Saudi Arabia, ⁵Geosciences Department, College of Science, United Arab Emirates University, Al Ain, United Arab Emirates, ⁶Economic Geology Research Centre (EGRU), College of Science and Engineering, James Cook University, Townsville, QLD, Australia, ⁷Environmental Sciences Department, Faculty of Science, Port Said University, Port Said, Egypt

This study evaluated concentrations, spatial distribution, and ecological-health risks of nine heavy metals in 25 surface sediment samples from Wadi Ghadir outlet, southeastern Red Sea coast, Egypt. The sediments were sandy (>94%), alkaline (pH 8.12), and contained moderate organic matter (5.6%-8.9%). Metal concentrations (mg/kg) followed: Fe > Ba > Cr > Zn > Ni > V > Pb > Cu > Co. Ba, Cr, and Ni exceeded Canadian soil quality guidelines and global Earth crust backgrounds, while others remained below. Spatially, Ba, Ni, and V peaked in the north, Co, Cr, and Zn in central sites, and Pb, Cu, and Fe in the south. Multivariate analyses indicated both natural and anthropogenic sources. Enrichment and contamination factors showed moderate enrichment for Pb and Ni, and considerable contamination for Ni. Geo-accumulation index ($I_{geo} > 5$) and pollution load index (PLI; 1.62) confirmed significant contamination. Ecological risk indices (PERI <150, Erⁱ <40) suggested overall low risk, with Ni and Pb most concerned. Additional sediment quality indices (MERMQ, TRI, mHQ) pointed to medium-moderate ecological and toxic risks, while human health evaluation revealed low non-carcinogenic and carcinogenic risks. Radiological analyses of ²³²Th, ⁴⁰K, and ²²⁶Ra revealed concentrations (Bq/Kg) and dose indices within global safety limits, indicating negligible radiological risk.

KEYWORDS

metal pollution, spatial pattern, radiological risk indices, sediment, Red Sea, South Egypt

1 Introduction

The Red Sea's coastal zones are vital for the blue economy, supporting fisheries, transport, mining, and tourism, while also delivering ecological services such as habitat provision, shoreline protection, and carbon storage through mangroves and coral reefs (Mohammed et al., 2024; Saleh et al., 2025). Egypt relies heavily on these resources for food, energy, and industry, making them central to both livelihoods and development (Al-Mur and Gad, 2022). However, human pressures—ranging from unregulated tourism to industrial expansion—are intensifying. These changes threaten fragile ecosystems,

particularly coral reefs, and highlight the urgency of balancing economic growth with environmental sustainability (Zhang et al., 2016; Abdelaal et al., 2022; 2024; Lasheen et al., 2024). The rapid expansion of tourism could pose significant risks to coral reef ecosystems. To evaluate and manage these pressures, researchers increasingly rely on ecological and human health risk assessments, which help identify contaminant levels, assess their potential impacts, and provide guidance for effective environmental management strategies (Mohammadi et al., 2019; Ardila et al., 2023; Wan et al., 2023).

Anthropogenic activities including mining, land reclamation, and recreational development have increased sediment disturbance and heavy metal inputs to Red Sea coastlines (Zhang et al., 2016; Abdelaal et al., 2022; 2024; Lasheen et al., 2024). Elevated concentrations of metals such as Ni, Cr, and Pb are often linked to both natural sources (e.g., mafic rocks) and anthropogenic discharges. These pollutants pose risks to marine life, bioaccumulate through food webs, and may affect human health. Previous studies have mapped contamination hotspots, yet site-specific assessments remain limited in some coastal outlets, leaving uncertainty about localized risks and contaminant sources.

In addition to heavy metals, coastal sediments may contain naturally occurring radioactive materials (NORMs), including isotopes of thorium, uranium, and potassium. These are enriched in heavy minerals such as zircon and monazite, which are abundant in Red Sea sediments due to erosion and transport processes (Al-Mur and Gad, 2022; Fathy et al., 2023; Khaleal et al., 2023a). Radiation exposure is influenced by geology, soil type, and cosmic activity, and can affect ecosystems and human health (UNSCEAR, 2000; Zakaly et al., 2024). While several studies have reported baseline radiation levels across the Red Sea (Al-Hamarneh and Awadallah, 2009; Lasheen et al., 2022), integration with metal contamination data is rare.

Research on Red Sea sediments has generally examined heavy metals and radiation independently, producing fragmented insights into ecological and health risks (Özden et al., 2023; Ravisankar et al., 2015). For example, some studies have documented elevated heavy metals linked to industrial effluents, while others focused on radiation mapping to estimate background dose rates (AlZahrani et al., 2011; Kumar et al., 2024). However, comprehensive evaluations that integrate trace metal contamination, radionuclide activity, and ecological–health risk assessments remain scarce. This gap limits the ability to identify combined hazards and hinders the development of holistic management strategies tailored to vulnerable coastal systems.

This study provides the first integrated assessment of heavy metals and natural radionuclides in sediments from Wadi Ghadir, a relatively unexplored locality along Egypt's southeastern Red Sea coast. Unlike earlier Red Sea studies, it combines multiple ecological, radiological, and health risk indices for a comprehensive evaluation. The sediments are economically important, with potential applications in tourism, infrastructure, and the nuclear industry. The research objectives are to: (1) quantify heavy metal contamination and potential sources using geochemical and statistical tools; (2) map spatial variability through GIS; (3) evaluate activity concentrations of ²³²Th, ²²⁶Ra, and ⁴⁰K and associated radiological risks; and (4) assess ecological and health implications. This integrated approach provides a more complete understanding of sediment-related hazards.

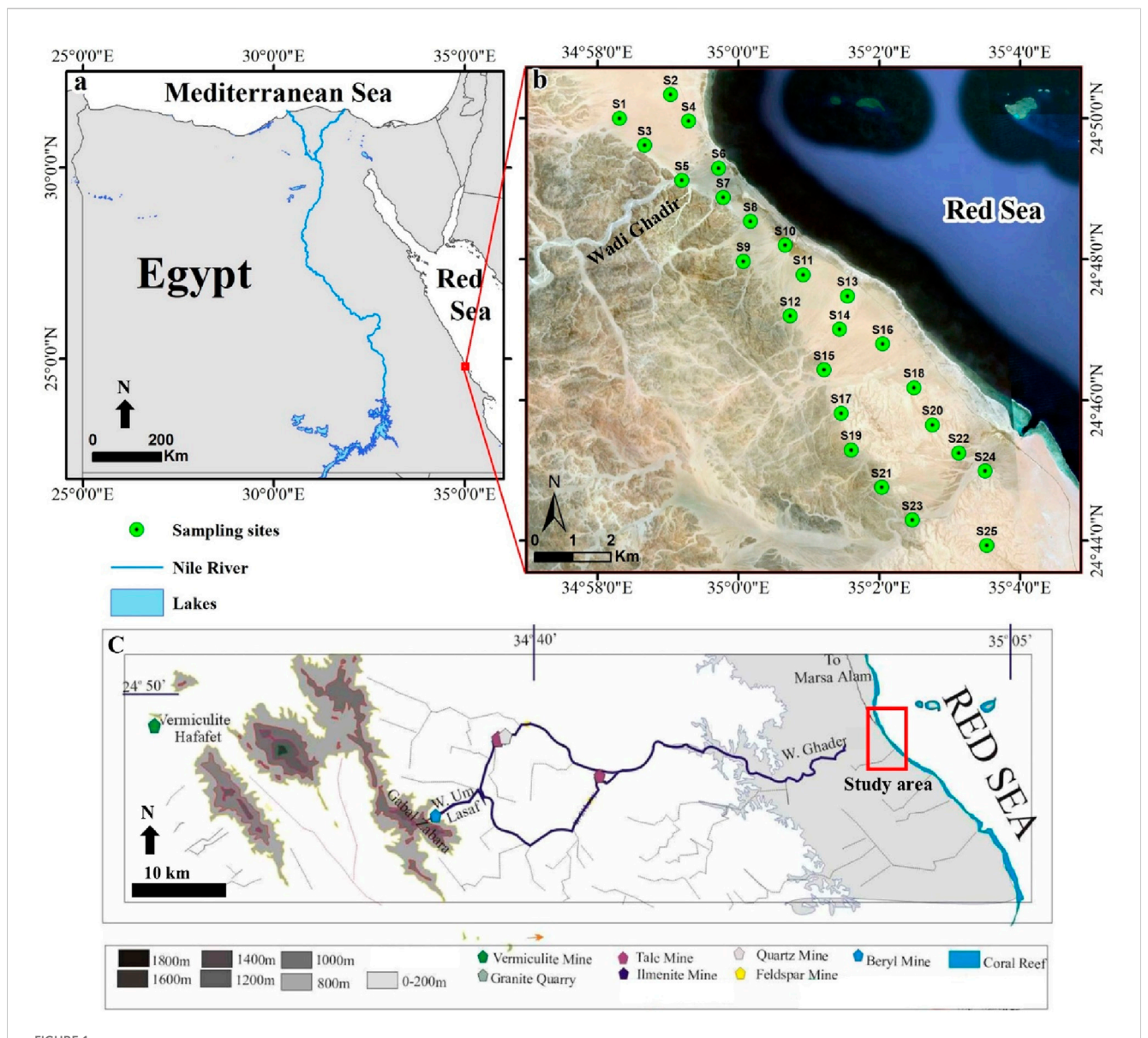
2 Materials and methods

2.1 Study area and geologic setting

Wadi (W.) Ghadir, located in the South Eastern Desert (SED) of Egypt at about 30 km south of Marsa Alam along the Red Sea shoreline (Figure 1). W. Ghadir is formed by fluvial and erosional processes, and is characterized by Precambrian basement rocks, which are part of the Arabian-Nubian Shield (Saleh et al., 2024). These rocks include ancient metamorphic and igneous formations such as gneisses, schists, granites, and volcanic rocks that were formed during the Pan-African orogeny (approximately 600-700 million years ago). The region features significant structural features such as faults and shear zones, influenced by the Red Sea Rift system. The tectonic activity along faults and shear zones has facilitated the emplacement of hydrothermal mineral deposits, making Wadi Ghadir a target for mineral exploration. The area also contains valuable mineral resources, including gold, rare metals and radioactive minerals, associated with its complex tectonic and magmatic history (Abdelaal et al., 2021; Kamar et al., 2021). Overlying the Precambrian basement rocks are Phanerozoic sedimentary deposits, including sandstones, limestones, and evaporites from the Cretaceous to Cenozoic periods. These sediments were deposited during various marine transgressions and regressions associated with the ongoing evolution of the Red Sea (Kamar et al., 2021). To illustrate sampling sites and distinct land/water features in the W. Ghadir outlet region along the Red Sea coast (Figure 1b), a Landsat-8 OLI satellite image was utilized (obtained from the U.S. Geological Survey (USGS) website: https://earthexplorer.usgs.gov/; Path: 173; Row: 43; acquisition date: 28 July 2024). The OLI image was processed using a composite bands tool, incorporating true-color bands (4, 3, and 2) to highlight the land use characteristics of the study area (Figure 1b) (Saleh et al., 2025; Lasheen et al., 2024; Saralioglu and Vatandaslar, 2022). In the present region, most of the coastal sediments consist of sand, gravels, and mud, exhibiting distinct ripple marks (Supplementary Figures S1a-f). These marks can be distinguished from one another based on their orientation, unique patterns, and external forms (Supplementary Figure S1d). Globally, mangrove ecosystems harbor highly valuable plants that produce a wealth of branches and various other organic materials. The mangrove environment is enriched by organic matter as it spreads to surrounding areas.

2.2 Sampling and analysis of sediments

Twenty-five sediment samples (S1-25) were collected from the top layer (0-20 cm) of W. Ghadir outlet in the Red Sea region (Figure 1b) using a hand-operated auger, to ensure adequate spatial coverage across the study area. The sampling sites were selected to represent different geomorphological settings and potential pollution sources, guided by previous assessments. This strategy provides a robust dataset, and the accompanying map clearly illustrates site distribution and labeling (Figure 1b). The samples were then transported to the lab in clean 1-kg containers for chemical analysis, including pH and total organic matter (TOM) measurements. Approximately 30 g of each sample underwent



(a) Location map for Wadi Ghadir outlet, Red Sea coastline, South Egypt, approximately 30 km south of Marsa Alam. (b) Landsat-8 true color image (bands: 4, 3, 2) displaying the study area's unique land/water features and coastal sediment sampling locations. (c) simplified topographic map showing the geological features (e.g., G. Zabara) and mining/ore sites (e.g., vermiculite, granite, talc, ilmenite, and beryl) of Wadi Ghadir at about 20 km to the west of the study area, that modified after (Mansour, 2003).

particle size analysis. The samples were treated with 15% $\rm H_2O_2$ and diluted HCl to remove carbonate and organic debris (Song et al., 2023). Sediment texture was classified using ternary diagrams (Folk, 1980), categorizing the samples based on grain size: gravel, sand, or mud (silt with clay) (Ardila et al., 2023). Sand and gravel fractions were analyzed using wet sieving, while the mud fraction was examined using the pipette method, following Folk's (1980) approach. Organic matter content was evaluated by heating 2 g sediment samples in a 550 °C furnace and measuring weight loss (Dean, 1974). The percentage of inorganic material was determined by post-procedure weighing, as described by Dean (1974). For metal analysis, the finest sediment fractions (<177 μ m) were prepared by grinding, screening, and air drying at room temperature, according to the method of (Haluschak, 2006). One-gram samples were

digested using nitric acid (HNO₃), perchloric acid (HClO₄), and hydrochloric acid (HCl), then filtered to remove any remaining material (Oregioni and Astone, 1984). Nine heavy metals (Ba, Co, Pb, Cu, Cr, Ni, Zn, V, and Fe) were extracted from the sediments using ICP-OES at the National Research Centre (NRC), Giza, Egypt, following Oregioni and Astone's (1984) protocol. The limits of detection (LODs) for Ba, Co, Pb, Cu, Cr, Ni, Zn, V, and Fe are 0.2, 0.2, 1, 1, 0.5, 1, 3, 0.1, and 10 mg/kg, respectively. The accuracy and precision of metal determinations were validated using certified external reference standards (SRM 2706 from NIST (USA) and Certipur from Merck Co. (Germany), yielding recovery rates between 90% and 99%. The ICP-OES operating conditions were systematically optimized to ensure maximum sensitivity to the target elements.

2.3 Ecological, SQGs and health risk assessment indices

This study involved the calculation and application of five ecological risk indices. Enrichment Factor (EF) (Zhang et al., 2016), calculated as $EF = (C_s/Fe_s)/(C_b/Fe_b)$, where C_s is the sample's analysed metal value, C_b is the metal crust background, and Feb is the Fe crust background (Supplementary Table S1). Background levels in the Earth's crust for Ba, Co, Pb, Cu, Cr, Ni, Zn, V, and Fe are 417, 12, 25, 26, 100, 20, 66, 100, and 50,000 mg/kg, respectively (Kabata-Pendias and Mukherjee, 2007). Contamination Factor (CF), calculated as CF = C₂/C_b (Hakanson, 1980), which is the result of dividing the detected metal concentration (Cs) in the sediments by local reference value (C_b) (Mahmoud et al., 2020). Index of Geo-accumulation (I_{geo}) calculated as $Igeo = log_2 \frac{Cn}{1.5*Bn}$, where B_n is the metal crust-background value and C_n is the investigated metal value. A normalizing factor of 1.5 is applied (Mueller, 1981) (Supplementary Table S1). Pollution Load Index (PLI) (Tomlinson et al., 1980), calculated as PLI = (CF1 * CF2 * CF3* ... * CFn)^{1/n}, where "n" denotes the number of metals analyzed (nine in this study), and "CF" denotes the contamination factor of the metals (Supplementary Table S1).

Potential Ecological Risk Index (PERI), calculated as PERI = $\sum_{i=1}^{n} \text{Er}_{i} = \sum_{i=1}^{n} \text{Tri} \times \text{CFi}$, where CF is the contamination factor, Tri is a metal's hazardous response factor (Co = 5, Pb = 5, Cu = 5, Cr = 2, Ni = 5, Zn = 1, V = 2, and Fe = 1), and Erⁱ is potential ecological risk factor (Hakanson, 1980) (Supplementary Table S1).

Additionally, three sediment quality guidelines (SQGs) were utilized, including the mean effects range median quotient (MERMQ), calculated as MERMQ = $\frac{\sum (Ci/ERMi)}{n}$, where Ci is the metal value that has been measured, ERMi is the metal's effects range-median, and n is the total number of metals that have been analyzed (Long et al., 2000; 1995) (Supplementary Table S1). Toxic Risk Index (TRI), calculated as TRIi = $\sqrt{\frac{(\frac{Ci}{TEL})^2+(\frac{Ci}{TEL})^2}{2}}$ and TRI = $\sum_{i=1}^n$ TRIi, where TRIi is the toxic risk index for a single element i and TRI indicates integrated metals in a sediment sample, are calculated using SQGs threshold effects level (TEL) and probable effects level (PEL) (Long and MacDonald, 1998) (Supplementary Table S1), and modified hazard quotient (mHQ), calculated as mHQ = $\sqrt{\frac{Ci}{TELi}} + \frac{Ci}{PELi} + \frac{Ci}{SELi}$, compares the metal value found in sediments to the SQG standards, namely, TEL, PEL, and severe effect level (SEL) (MacDonald et al., 2000). Furthermore, two human health risk indices were calculated: the non-carcinogenic Hazard Index (HI) is calculated as HI = $\sum_{i=1}^{n} HQi$, HQ = CDI/RfD, and CDI_{dermal} = $(Cs \times CF \times SA \times AF \times ABS \times EF \times ED)/(BW \times AT)$ (Supplementary Table S2), and The RfD values for Ba, Co, Pb, Cu, Cr, Ni, and Zn are 0.0049, 0.02, 0.003, 0.0371, 0.015, 0.02, and 0.3, respectively (Miletić et al., 2023; U.S. EPA, 2007; 2005). Total Cancer Risk (TCR) (RAIS, 2017; U.S. EPA, 2002), calculated as TCR = $\sum CR$ and CR = $CDI_{dermal} \times CSF$, where the cancer slope factor (CSF) values for Pb, Cr, and Ni that were applied in this study are 0.042, 41, and 0.91, respectively, according to (OEHHA, 2023). The input data and equations of the employed ecological, SQGs, and health risk indices are reported in the Supplementary Material, Supplementary Tables S1 and S2.

2.4 Radioactivity indices in sediments

To evaluate the radiological impact of sediment samples, it is necessary to calculate various radiological parameters. These include

absorbed dose rates (D_{air}), their annual outdoor and indoor effects (AED_{out} and AED_{in}), gamma index (I_{γ}), external and internal indexes (H_{in} and H_{ex}), excess life cancer risk (ELCR), alpha index (I_{α}), and radium equivalent (Ra_{eq}). The radionuclides ⁴⁰K, ²²⁶Ra, and ²³²Th (Bq/Kg) are denoted by C_{K} , C_{Ra} , and C_{Th} , respectively. Detailed equations for assessing different radiation exposure and risk factors can be found in Supplementary Table S3.

The collected sediment samples underwent a preparation process. Initially, they were air-dried before being divided. Representative samples then had their heavy minerals extracted using the bromoform heavy liquid extraction technique. Following this, the samples were subjected to magnetic separation using a Frantz isodynamic separator, which categorized them according to their distinct magnetic characteristics. The extracted minerals were subsequently analyzed at the Nuclear Materials Authority laboratories. An Environmental Scanning Electron Microscope (ESEM, Phillips XL-30) was employed for identification, with confirmation provided by a binocular microscope.

2.5 Statistical analysis

Various statistical techniques were utilized to assess potential sources of metals in the sediments, using Statgraphics software (Ver. 18). These methods encompassed descriptive statistics, Pearson correlation analysis, factor analysis (FA), and cluster analysis (Reimann et al., 2008). To assess the normality of the data set, different statistical methods were employed. The Kolmogorov-Smirnov test was utilized to evaluate the normal distribution of pH, organic matter, and the metals under investigation. For the grain size dataset, skewness and kurtosis were analyzed. The analysis revealed that all datasets fell within the expected range for normal distribution (Table 1).

3 Results and discussions

3.1 Sediment's composition and type

Supplementary Tables S4 and S5 display the analyzed results of grain size, pH, and total organic matter (TOM), with Table 2 showing a summary and Figure 2 illustrating the spatial distribution. The sediments at W. Ghadir outlet showed the smallest average percentages of gravel (0.87%) and mud (silt + clay; 4.85%), while sand constituted the bulk (>94.16%) of the sediment composition (Figure 2a; Supplementary Table S4). The outlet sediments of W. Ghadir were found to be alkaline (pH = 8.12) with TOM levels ranging from low to moderate (5.6%-8.9%) (Ercegovac and Kostić, 2006) (Table 1). This composition could be linked to the mangrove swamps along the W. Ghadir coastline, which supply organic matter through fallen leaves and debris (Figure 2b). The sediment sites exhibited varying patterns of pH and organic matter content (Figures 1b, 2b). Southern locations (e.g., S18 and S21) had the highest proportions of gravel and sand, possibly due to substantial fluvial deposits from western wadies that regularly flood into the Red Sea (Figures 1b, 2a). In contrast, central sites (e.g., S10), where mangrove swamps are

TABLE 1 Summary statistics of metals contents (mg/kg), grain size (%), pH, and organic matter in coastal sediments of W. Ghadir outlet, Red Sea.

n = 25	Ва	Со	Pb	Cu	Cr	Ni	Zn	V	Fe	Gravel %	Sand %	Silt + Clay%	рН	TOM %
Mean	488.96	7.64	52.96	41.72	173.48	86.64	112.24	85.88	51,513	0.87	94.16	4.85	8.12	7.66
Min	158	3	15	11	56	23	24	33	36,649	0.2	91.7	2.5	7.6	5.6
Max	1,025	14	102	92	366	165	245	145	72,388	1.5	96.6	7.7	8.8	8.9
Median	456	7	47	37	164	78	78	82	52,245	0.9	93.9	5.1	8.1	7.8
SD	245.9	3.14	27	21.96	71.6	41	74.73	28.26	7,728	0.37	1.32	1.3	0.35	0.87
CV%	50.3	41.1	51	52.6	41.2	47.4	66.5	33	15	42.6	1.4	26.2	4.3	11.3
Skewness	0.71	0.68	0.51	1.45	1.99	0.81	1.5	0.46	0.45	-0.23	0.10	0.23	0.68	-2.00
Kurtosis	-0.97	-0.64	-1.24	-0.10	1.35	-0.64	-0.85	-0.47	1.35	-1.13	-0.79	-0.58	-0.85	0.46
CSQG (2007)	750	40	70	63	64	50	200	130	-					
Turekian and Wedepohl (1961)	-	19	20	45	90	68	95	130	47,200					

Bold face relates to the highest and significant values.

TABLE 2 The average metal' contents (mg/kg) in coastal sediments of W. Ghadir were compared to those found in Egyptian and global coastal sediments. Boldface relates to the highest values of metals.

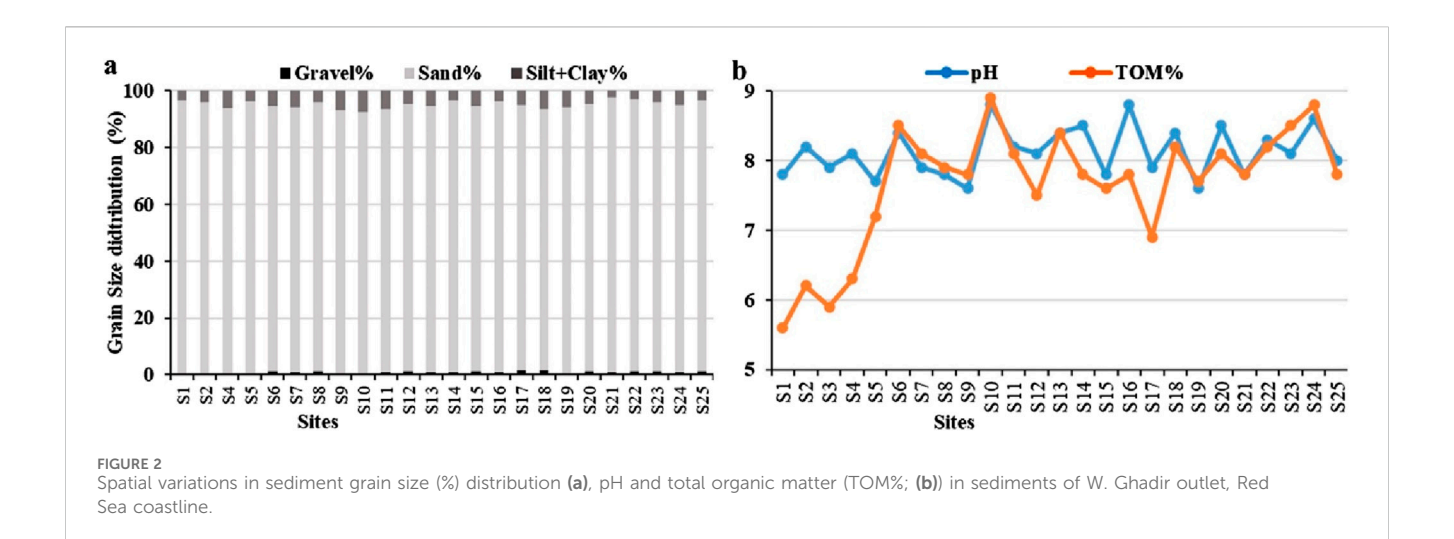
Location	Ва	Со	Pb	Cu	Cr	Ni	Zn	V	Fe	References
W. Ghadir outlet, Red Sea, Egypt	488.96	7.64	52.96	41.72	173.48	86.64	112.24	85.88	51,513	This study
Sharm El Luli, Red Sea, Egypt	304.15	34.12	85.94	38.15	162	37.47	124.78	260.52	44.765	Saleh et al. (2025)
Red Sea coastline, Egypt	171.84	4.81	4.89	7.7	53.84	15.37	27.55	29.78	14,562	Badawy et al. (2018)
W. El-Gemal outlet, Red Sea, Egypt	-	1.24	2.57	0.47	-	2.44	6.74	-	4,618	Al-Kahtany et al. (2023)
W. El-Gemal Island, Red Sea, Egypt	-	2.05	0.84	0.31	-	0.7	3.4	-	1,271	Lasheen et al. (2024)
Abu Minqar Island, Red Sea, Egypt	-	2.34	1.19	0.27	-	0.76	2.89	-	921	Abdelaal et al. (2024)
Marsa Alam coast, Red Sea, Egypt	-	1.83	2.23	1.94	10.62	6.82	28.83	-	1,674	Farhat et al. (2022)
Gulf of Suez, Egypt	-	7.4	2.78	1.66	8.98	5.58	3.96	-	540	Nour et al. (2022)
Ras Abu Ali Island, Saudi Arabia	-	1.43	3.5	4.14	7.86	13	6.9	6.67	4,808	Al-Kahtany and El-Sorogy (2023)
Aqaba coast, Red Sea, Saudi Arabia	-	4.5	6.6	30	39	14	24	-	3,374	El-Sorogy et al. (2020)
Northeast coast, Iran	142	8	9	13	70	50	34	41	21,800	Vaezi and Lak (2023)
Lagoon lakes, Turkey	-	-	17.74	11.63	90.80	25.04	19.43	-	28,191	Yüksel and Fikret (2025)
Vedaranyam coast, India	-	71	-	115.1	48.8	66	623	-	65,966	Gopal et al. (2023)
Zhejiang coast, China	457.4	17.17	29.4	28.15	55.46	45	115.87	142.8	-	Zhao et al. (2023)
Mailiao coast, Taiwan	-	-	21.69	30.96	86.1	51.65	174.12	-	38,370	Fang and Chang (2023)

Bold face relates to the highest and significant values.

located, showed the highest levels of mud, pH, and organic matter (Figures 1b, 2).

3.2 Metal's contents, patterns, and potential sources

The heavy metal concentrations in coastal sediments of the Red Sea's W. Ghadir outlet are detailed in Supplementary Table S5. Table 1 summarizes these metals, while Figure 3 illustrates their spatial distribution across sampling sites (S1-25). The observed metal concentrations aligned with Canadian soil quality guidelines (CSQG, 2007) and Earth's sedimentary rocks (shales) (Turekian and Wedepohl, 1961), as shown in Table 1. The analyzed metals, ranked by concentration (mg/kg), were Fe (51,513) > Ba (488.96) > Cr (173.48) > Zn (112.24) > Ni (86.64) > V (85.88) > Pb (52.96) > Cu (41.72) > Co (7.64) (Table 1). In this study, Cr, Ni, and Fe exhibited higher levels compared to Earth's sedimentary rocks



(shales) (Turekian and Wedepohl, 1961) and Canadian guidelines (CSQG, 2007). This enrichment is linked to the basement rocks and mining activities in W. Ghadir that cross alteration zones containing various mineral deposits (e.g., vermiculite, granite, talc, ilmenite, and beryl) at about 20 km to the west of study area (Figure 1c). During floods, these wadies transport minerals from upstream rocks to downstream mangrove areas, resulting in mineral deposition (Mohammed et al., 2024). Conversely, the other metals examined (Ba, Co, Cu, Zn, and V concentrations were lower than Canadian guidelines (CSQG, 2007).

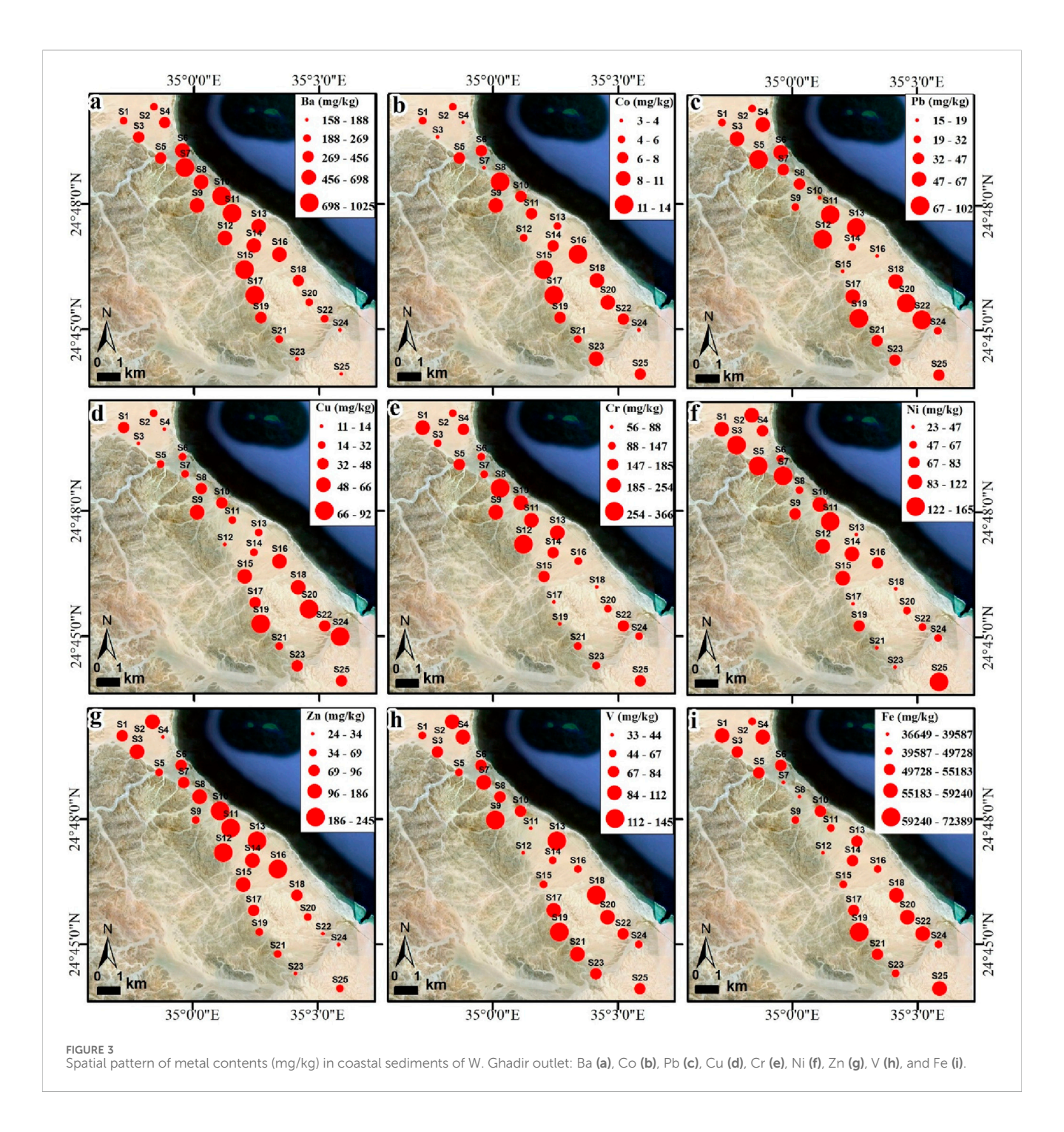
In respect to the spatial distribution, the northern sediment sites (e.g., S1-10) of W. Ghadir outlet showed the highest contents of Ni (Figure 3f). The central sites (e.g., S11-15) displayed the highest contents of Ba (Figure 3Aa), Co (Figure 3b), Cr (Figure 3e), Zn (Figure 3g), and V (Figure 3h), coinciding with significant wadi discharge fluvial deposits and frequent W. Ghadir flooding (Figures 1b, 4). While the southern sites (e.g., S17-25) had the highest Pb (Figure 3c), Cu (Figure 3d) and Fe (Figure 3i). That could be referred to anthropogenic and tourist-related activities (Figure 1b).

Table 2 compares the mean metal contents in W. Ghadir sediments with those of Egyptian and global coastal sediments. The W. Ghadir average Ba, Cr, and Ni contents surpassed those found in Egypt's and other countries' coastal sediments (Al-Kahtany et al., 2023; Badawy et al., 2018; Nour et al., 2022; Yüksel and Fikret, 2025) (Table 2). However, the average contents of Co, Pb, Cu, Zn, V, and Fe in this study were lower than those in Sharm El Luli, Red Sea, Egypt, India and China's coastal sediments (Gopal et al., 2023; Fang and Chang, 2023; Saleh et al., 2025) (Table 2).

Analysis of 25 sediment samples from the W. Ghadir outlet along the Red Sea coast revealed strong Pearson's correlations between heavy metals and various parameters, including organic matter, pH, and particle size (Table 3). Notably, moderate positive correlations were identified between Ba and Zn (r = 0.55; p < 0.01), Ba and Mud% (r = 0.47; p < 0.05), Co and Cu (r = 0.41; p < 0.05), Co and Gravel% (r = 0.51; p < 0.01), TOM% and pH (r = 0.46; p < 0.05), and V and Fe (r = 0.48; p < 0.05) (Table 3). Conversely, significant negative correlations were observed between Fe and Ba (r = -0.53; p < 0.01), Cr (r = -0.51; p < 0.01), and Zn (r = -0.41; p < 0.05), as well as between Ba and Sand% (r = -0.48; p < 0.05) (Table 3). It is noteworthy that Pb did not show

any significant correlation with other metals or sediment parameters, suggesting a distinct source or behavior compared to the other analyzed elements.

The suitability of the data set for the Factor analysis (FA) was confirmed by the Kaiser-Meyer-Olkin (KMO) test (overall value = 0.77) and Bartlett's test of sphericity ($\chi^2 = 275.2$, df = 25, p < 0.05), indicating adequate intercorrelations among variables. The FA results of investigated metals in W. Ghadir sediments revealed three distinct factors (Figure 4; Supplementary Table S6). The first factor (F1) explained 21.1% of the total data variance, exhibiting positive significant loadings for Pb, Cr, and Zn, while showing negative loadings for V and Fe (Figure 4a). This pattern suggests that F1 may reflect anthropogenic influences, particularly from industrial, urban, or transportation-related sources such as fuel combustion, metal processing, and waste discharge. Pb, Cr, and Zn are commonly associated with vehicular emissions, batteries, and industrial effluents. In contrast, the negative loadings of V and Fe-typically of natural origin-may indicate dilution or displacement of natural geogenic signatures by human-induced contamination. Thus, F1 likely represents a mixed anthropogenic pollution factor. F2 accounted for 18.2% of data variance, with positive significant loadings for Co, Cu, Gravel%, TOM%, and pH, and negative loadings for Ni (Figure 4a). This suggests influence from both natural and anthropogenic sources. Co and Cu may originate from weathering of mafic rocks or mineralization mining sites west to the study area (Figure 1c), while the association with TOM% and pH points to organic complexation processes in coarse sediments. Overall, F2 highlights mixed geogenic and anthropogenic contributions, where natural rock weathering interacts with human activities to shape metal distributions. The contrasting Ni behavior underscores heterogeneous geochemical controls and possible selective retention or mechanisms within the sediment matrix. transport F3 contributed 18.1% of the overall data variation, with significant positive loadings for Ba% and Mud%, and negative loadings for Sand% (Figure 4a; Supplementary Table S6). This suggests that F3 may represent fine-grained sediment accumulation zones influenced by terrestrial runoff or lowenergy depositional environments where barium tends to concentrate with finer particles. Potential sources include



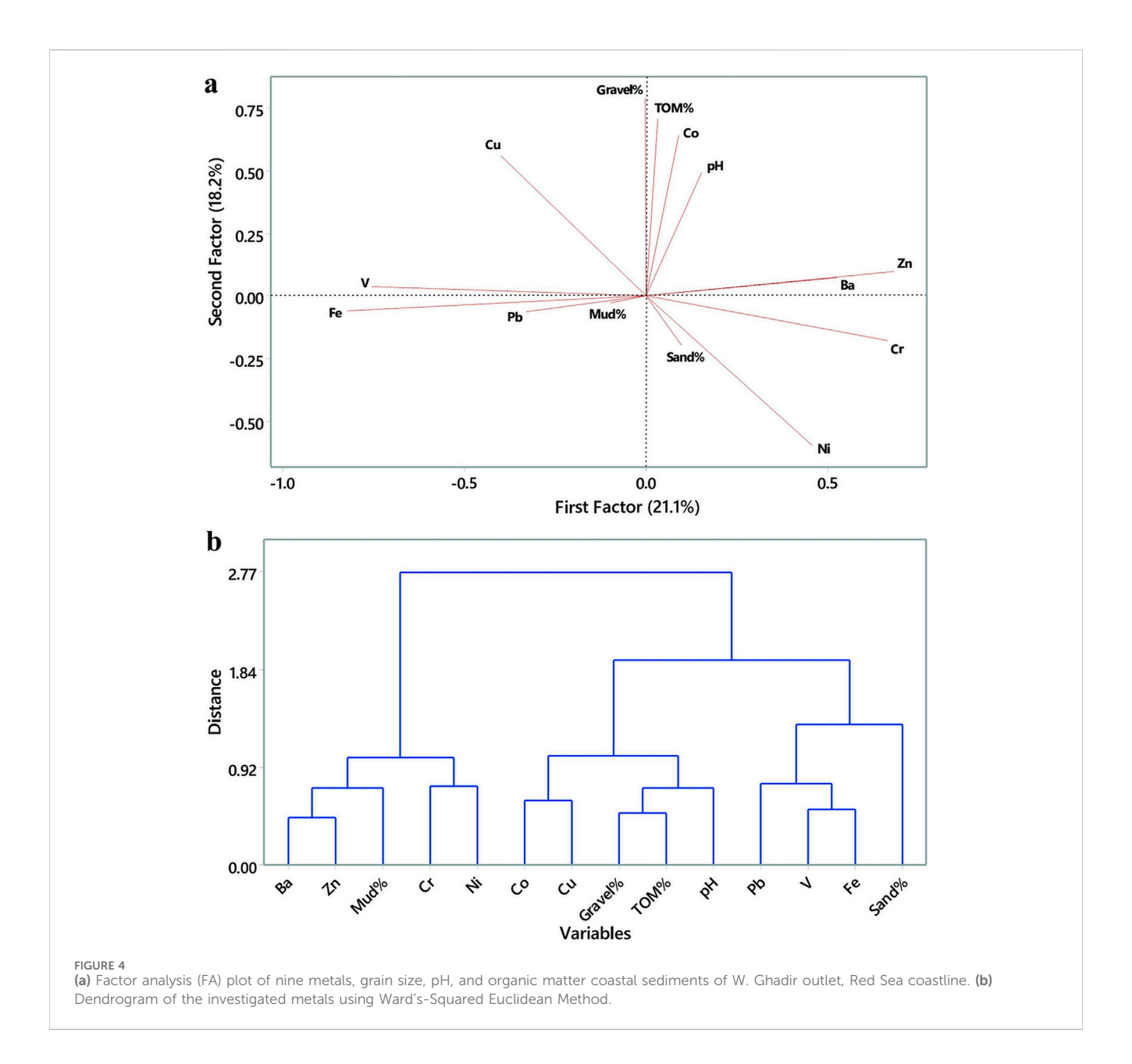
weathering of feldspar-rich rocks, or inputs from urban or agricultural runoff. The negative association with sand implies a shift from high-energy conditions, such as coastal currents or wave action, to more quiescent areas that favor mud and associated metal accumulation.

Cluster analysis of sediment characteristics and metal concentrations at the W. Ghadir outlet, using the Ward's method with squared Euclidean distance, revealed three distinct clusters (Figure 4b). The first group includes Pb, V, Fe, and Sand%, the second comprises Co, Cu, pH, Gravel%, and TOM%, while the third consists of Ba, Cr, Ni, Zn, and Mud% (Figure 4b). Clustering suggests shared sources or geochemical behaviors: Cluster

1 relates to mineral inputs, Cluster 2 reflects organic or coarse sediment associations, and Cluster 3 links fine particles with potentially anthropogenic metals.

3.3 Metal pollution risk assessment

The ecological enrichment factors (EFs) of metals in the coastal sediments of W. Ghadir are summarized in Supplementary Table S7 and illustrated in Figure 5a. The average EF across all metals was 1.78, ranging from 0.22 to 10.38. As shown in Figure 5a, Ni recorded the highest average EF (4.4), followed by Pb (2.06), both indicating



moderate enrichment (EF = 2-5). In contrast, Ba, Cu, Cr, and Zn showed minimal enrichment levels (EF = 1-2), while the mean EFs for Co and V suggested concentrations close to natural background levels (EF < 1) (Abdelaal et al., 2024; Lasheen et al., 2024; Saleh et al., 2025).

Figure 5b and Supplementary Table S8 present the calculated ecological contamination factors (CFs) for metals in the coastal sediments of W. Ghadir. As illustrated in Figure 5b, the average CFs follow the descending order: Ni (4.33) > Pb (2.12) > Cr (1.73) > Zn (1.70) > Cu (1.60) > Ba (1.17) > Fe (1.03) > V (0.86) > Co (0.64). Ni exhibited the highest mean CF, indicating considerable contamination (3 \leq CF < 6). Moderate contamination levels (1 \leq CF < 3) were observed for Ba, Pb, Cu, Cr, Zn, and Fe, suggesting that, in addition to nearby mining operations, anthropogenic (tourism-related) activities along the W. Ghadir coastline may be contributing to metal pollution. In contrast, Co and V displayed low contamination levels (CF < 1) (Abdelaal et al., 2024; Hakanson, 1980; Lasheen et al., 2024).

The geo-accumulation index ($I_{\rm geo}$) values for various metals in the coastal sediments of W. Ghadir are shown in Figure 5c and Supplementary Table S9. The metals are ranked in descending order of $I_{\rm geo}$ as follows: Fe (30.66) > Ba (16.85) > Cr (13.38) > V (12.40) > Zn (11.94) > Ni (9.99) > Pb (9.57) > Cu (9.29) > Co (5.80). $I_{\rm geo}$ values for all metals ranged from 4.58 to 31.17, with a mean of 13.32 (Figure 5c). According to Mueller's classification (1981) (Supplementary Table S1), this average place the sediments in class 7 ($I_{\rm geo}$ > 5), indicating extreme contamination (Mueller, 1981).

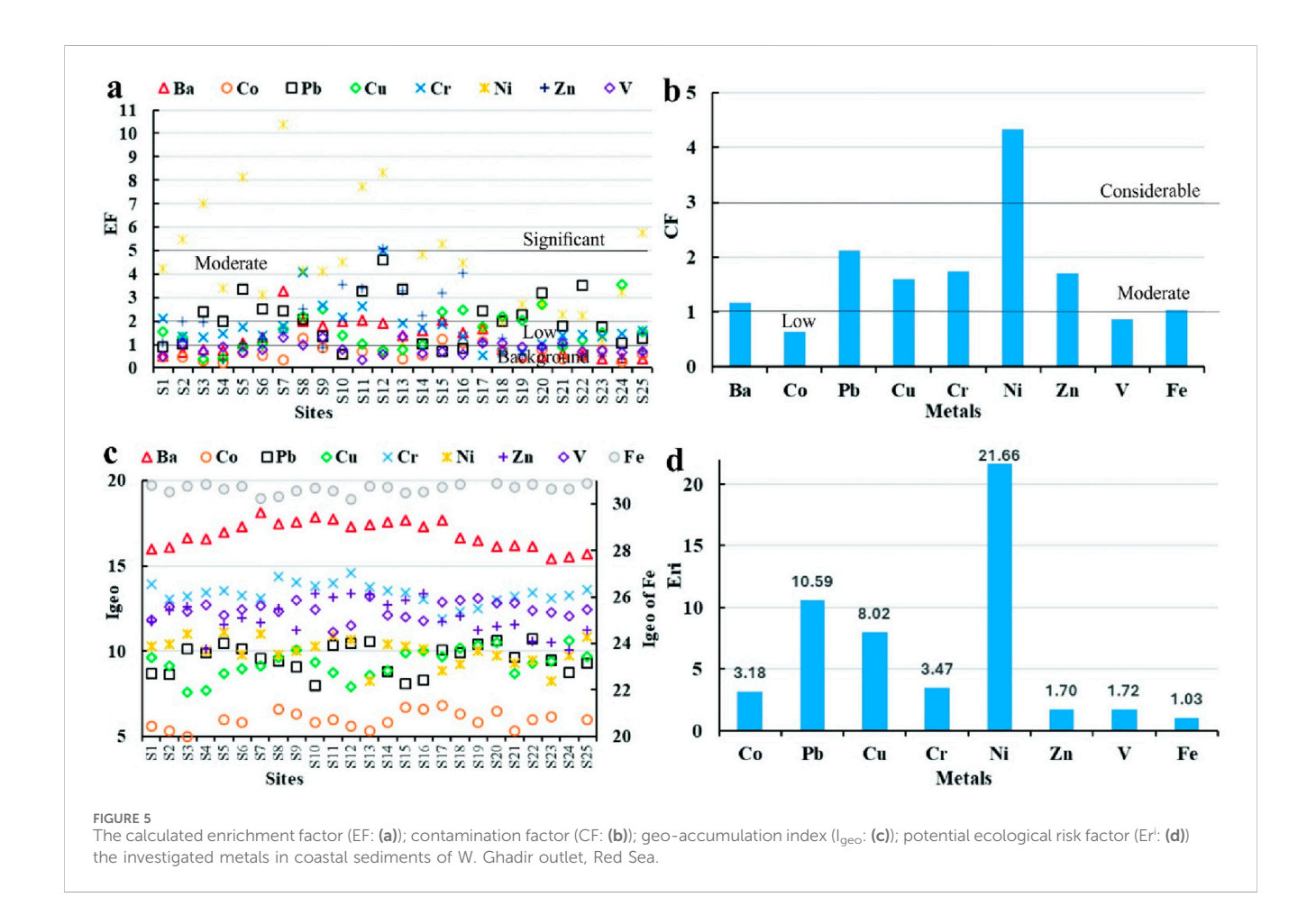
Supplementary Table S8 presents the Pollution Load Index (PLI) for the studied metals extracted from the coastal sediments of W. Ghadir. The calculated PLI value for all nine metals is 1.62 (Supplementary Table S8), indicating progressive contamination (PLI >1) according to (Hakanson, 1980). These findings suggest that the sediments are significantly polluted, likely due to the input of metal-rich discharges carried by W. Ghadir into the coastal environment (Mohammed et al., 2024) (Figure 1c).

TABLE 3 Pearson correlations within sediment particle size, pH, organic matter, and examined metals in coastal sediments of W. Ghadir outlet, Red Sea.

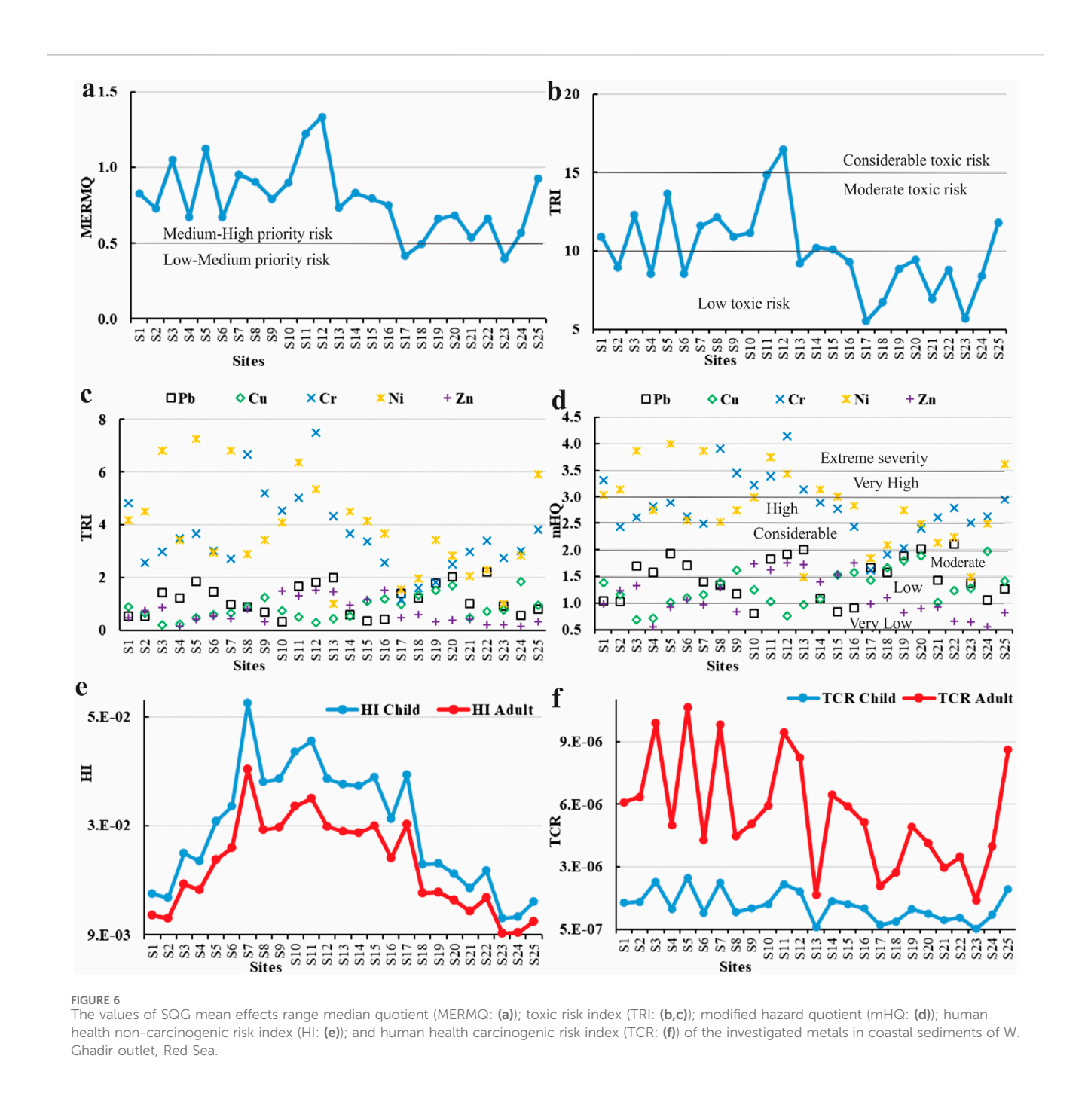
	Ва	Со	Pb	Cu	Cr	Ni	Zn	V	Fe	Gravel%	Sand%	Mud%	рН	TOM%
Ва	1													
Со	0.21	1												
Pb	-0.13	-0.05	1											
Cu	-0.23	0.41ª	-0.19	1										
Cr	0.25	-0.07	-0.01	-0.33	1									
Ni	0.25	-0.28	-0.05	-0.33	0.26	1								
Zn	0.55 ^b	0.14	-0.11	-0.31	0.41ª	0.19	1							
V	-0.07	-0.03	0.25	0.19	-0.41ª	-0.50 ^a	-0.31	1						
Fe	-0.53 ^b	-0.05	0.33	0.26	-0.51 ^b	-0.27	-0.41 ^a	0.48 ^a	1					
Gravel%	0.07	0.51 ^b	0.23	0.23	-0.12	-0.38	-0.02	0.03	-0.09	1				
Sand%	-0.48 ^a	-0.11	-0.08	-0.17	0.01	0.05	-0.20	-0.24	0.02	-0.20	1			
Mud%	0.47 ^a	-0.03	0.01	0.10	0.02	0.05	0.21	0.23	-0.08	-0.08	-0.96ª	1		
pН	0.02	-0.05	-0.10	0.13	-0.12	-0.23	0.38	-0.16	-0.08	0.21	-0.17	0.11	1	
TOM%	0.22	0.15	0.06	0.33	0.01	-0.33	0.10	0.08	-0.08	0.51 ^b	-0.35	0.20	0.46 ^a	1

 $^{^{\}mathrm{a}}$ Correlation is significant at <0.05 level.

Bold face relates to the highest and significant values.



^bCorrelation is significant at <0.01 level.



To evaluate metal concentrations in the coastal sediments of W. Ghadir, the Potential Ecological Risk Index (PERI) and individual risk factor (Er¹) were applied in this study, following the method of (Hakanson, 1980). The results are presented in Supplementary Table S8 and Figure 5d. The metals were ranked by Eri values as follows: Ni (21.66) > Pb (10.59) > Cu (8.02) > Cr (3.47) > Co (3.18) > V (1.72) > Zn (1.70) > Fe (1.03) (Figure 5d). On average, all metals posed a low ecological risk (Eri <40), although certain locations—such as site S5—showed moderate risk levels ($40 \le \text{Eri} < 80$) (Figure 5d). The overall PERI value for all metals was 44.29, which is less than the PERI value (68.4) estimated in Sharm El-Luli coastal sediments, Red Sea (Saleh et al., 2025), also indicating a low ecological risk

(PERI <150) (Abdelaal et al., 2024; Zhao et al., 2023; Saleh et al., 2025) (Supplementary Table S8).

Supplementary Table S10 and Figure 6a present the calculated Mean Effects Range-Median Quotient (MERMQ) values for metals in W. Ghadir coastal sediments, based on the Effects Range-Low (ERL) and Effects Range-Median (ERM) criteria outlined by Long et al. (1995); (2000). Table 4 compares sediment metal concentrations—specifically Pb, Cu, Cr, Ni, and Zn—with sediment quality guidelines (SQGs), including ERL, ERM, Threshold Effect Level (TEL), and Probable Effect Level (PEL). The results show that 12% of sites (3 out of 25) exceed the Pb PEL of 91.3 mg/kg, while 88% (22 out of 25) surpass the Cr PEL of 90 mg/kg. Notably, 80% of sites (20 out of 25)

TABLE 4 Metal values in coastal sediments of W. Ghadir outlet, compared to the SQGs ERL, ERM, TEL, and PEL levels (Long et al., 2000; 1995; Macdonald et al., 1996).

SQGs	Pb	Cu	Cr	Ni	Zn
ERL (mg/kg)	46.7	34	81	20.9	150
ERM (mg/kg)	218	270	370	51.6	410
TEL (mg/kg)	35	35.7	37.3	18	123
PEL (mg/kg)	91.3	197	90	36	315
Content range (mg/kg)	15-102	11-92	56-366	23-165	24-245
<erl%< td=""><td>48</td><td>44</td><td>8</td><td>0</td><td>72</td></erl%<>	48	44	8	0	72
ERL-ERM%	52	56	92	20	28
>ERM%	0	0	0	80	0
<tel%< td=""><td>32</td><td>44</td><td>0</td><td>0</td><td>64</td></tel%<>	32	44	0	0	64
TEL-PEL%	15	56	12	12	36
>PEL%	12	0	88	88	0

Bold face relates to the highest and significant values.

exceed the Ni ERM value of 51.6 mg/kg, and 88% (22 sites) exceed the Ni PEL of 36 mg/kg. In contrast, Cu and Zn concentrations remain below their respective ERM and PEL thresholds. The MERMQ values for Pb, Cu, Cr, Ni, and Zn range from 0.4 to 1.33, with an average of 0.79, indicating a medium-high priority risk level (0.51 < MERMQ \leq 1.5) (Figure 6a; Supplementary Table S10).

The estimated Toxic risk index (TRI) values for Pb, Cu, Cr, Ni, and Zn in W. Ghadir coastal sediments are shown in Supplementary Table S11 and Figures 6b,c present data based on the sediment quality guidelines (SQGs), specifically the Threshold Effect Level (TEL) and Probable Effect Level (PEL) criteria (Long et al., 2000; 1995). The average multi-element Toxic Risk Index (TRI) values across sediment sites ranged from 5.52 to 16.48, with an overall mean of 10.04 (Figure 6b), indicating a moderate toxic risk level (10 < TRI ≤15). Additionally, the average TRI values for individual metals followed the descending order: Ni (3.81), Cr (3.56), Pb (1.15), Cu (0.84), and Zn (0.69) (Zhang et al., 2016) (Figure 6c).

Supplementary Table S12 and Figure 6d present the calculated modified hazard quotient (mHQ) values for metals in the sediments of W. Ghadir, based on the Sediment Quality Guidelines (SQGs), including the Threshold Effect Level (TEL), Probable Effect Level (PEL), and Severe Effect Level (SEL) (Benson et al., 2018; Long et al., 2000; 1995). The average mHQ values for the metals ranged from 0.55 to 4.15, with an overall mean of 1.9, indicating moderate contamination severity $(1.5 \le \text{mHQ} < 2.0)$ (Figure 6d). The average mHQ values for individual metals were ranked in the following order: Ni (2.81) > Cr (2.80) > Pb (1.47) > Cu (1.28) > Zn (1.12) (Figure 6d). Pb, Cu, and Zn exhibited low contamination severity $(1.0 \le \text{mHQ} < 1.5)$, whereas Ni and Cr showed high contamination severity $(2.5 \le \text{mHQ} < 3.0)$ (Figure 6d).

The calculated non-carcinogenic hazard index (HI) values for metals in the W. Ghadir coastal sediments are presented in Supplementary Table S13 and Figure 6e. The HI values for both adults and children were determined based on the hazard quotient (HQ), reference dose (RfD), and chronic daily intake *via* dermal

exposure (CDI $_{Dermal}$) for each metal (RAIS, 2017; U.S. EPA, 2002; 1989). As shown in Supplementary Table S13, barium (Ba) exhibited the highest HQ values for both children (4.49×10^{-2}) and adults (3.43×10^{-2}) . However, the HQ values for all metals remained below the acceptable threshold (HQ < 1). The HI values for adults ranged from 9.21×10^{-3} to 3.93×10^{-2} , with an average of 2.18×10^{-2} , which is higher than 1.54×10^{-4} in Wadi El-Gemal coastal sediments (Al-Kahtany et al., 2023) and 1.71 \times 10⁻² in Sharm El-Luli coastal sediments, Red Sea (Saleh et al., 2025), while children's HI values ranged from 1.21×10^{-2} to $5.15 \times 12.24 \ 0^{-2}$, averaging 2.85×10^{-2} (Figure 6e), which is higher than 7.18×10^{-4} and 2.24×10^{-2} in Wadi El-Gemal and Sharm El-Luli coastal sediments, Red Sea, respectively (Al-Kahtany et al., 2023; Saleh et al., 2025). Overall, the HI values indicate no significant chronic non-carcinogenic health risk (HI < 1) from exposure to metals in the W. Ghadir sediments (Abdelaal et al., 2024; Emenike et al., 2020; Jalali et al., 2023; Lasheen et al., 2024; Saleh et al., 2025).

Supplementary Table S14 and Figure 6f present total cancer risk (TCR) estimates for adults and children exposed to Cd, Pb, and Ni in W. Ghadir coastal sediments, using cancer risk (CR), cancer slope factor (CSF), and chronic daily intake (CDI_{Dermal}) (U.S. EPA, 2007; 2005; 2002). Although Ni showed the highest CR (1.06 \times 10⁻⁶), all values remained below the permissible limit of 1×10^{-6} for individual metals (RAIS, 2017; U.S. EPA, 2002). Mean TCR values for children ranged from 4.78 $\times~10^{-7}$ to 2.91 $\times~10^{-6}$ (average: 1.57×10^{-6}), which exceeds 1.52×10^{-8} and 2.56×10^{-7} in Wadi El-Gemal and Sharm El-Luli coastal sediments, respectively (Al-Kahtany et al., 2023; Saleh et al., 2025). While adult values ranged from 1.83×10^{-6} to 1.11×10^{-5} (average: 5.99×10^{-6}) (Figure 6f), which is above 3.25×10^{-9} and 9.76×10^{-7} in Wadi El-Gemal and Sharm El-Luli coastal sediments, respectively (Al-Kahtany et al., 2023; Saleh et al., 2025). All values fell within the acceptable risk threshold of 1 × 10⁻⁴. TCR is a key indicator for evaluating potential cancer risk from prolonged exposure to hazardous metals like Pb, Cr, and Ni in sediments (Abdelaal et al., 2024; Emenike et al., 2020; Lasheen et al., 2024; Xu et al., 2022; Saleh et al., 2025).

The contamination patterns observed in W. Ghadir coastal sediments highlight clear ecological implications. Although the enrichment (EF), contamination factor (CF), and geoaccumulation index (Igeo) results suggest different levels of contamination, these variations reflect methodological differences rather than contradictions. EF and CF, which are normalized against background values, indicated moderate enrichment and considerable contamination primarily for Ni and Pb, suggest significant input from both natural (weathering of mafic and heavy mineral-rich rocks) and anthropogenic sources, including nearby mining activities and tourism-related discharges, with other metals remaining low to moderate, consistent with localized anthropogenic inputs from mining and tourism (Saleh et al., 2025). In contrast, the $I_{\rm geo}$ values classified the sediments as extremely contaminated (I_{geo} > 5), but this may overestimate pollution because it is highly sensitive to the choice of background reference (Mueller, 1981). The PLI value (1.62) further confirmed progressive contamination, aligning with CF and EF outcomes. Risk-based indices, however, presented a more conservative picture: the ecological risk factor (Erⁱ < 40) and PERI (<150) classified the sediments as low-risk overall, though Ni and Pb

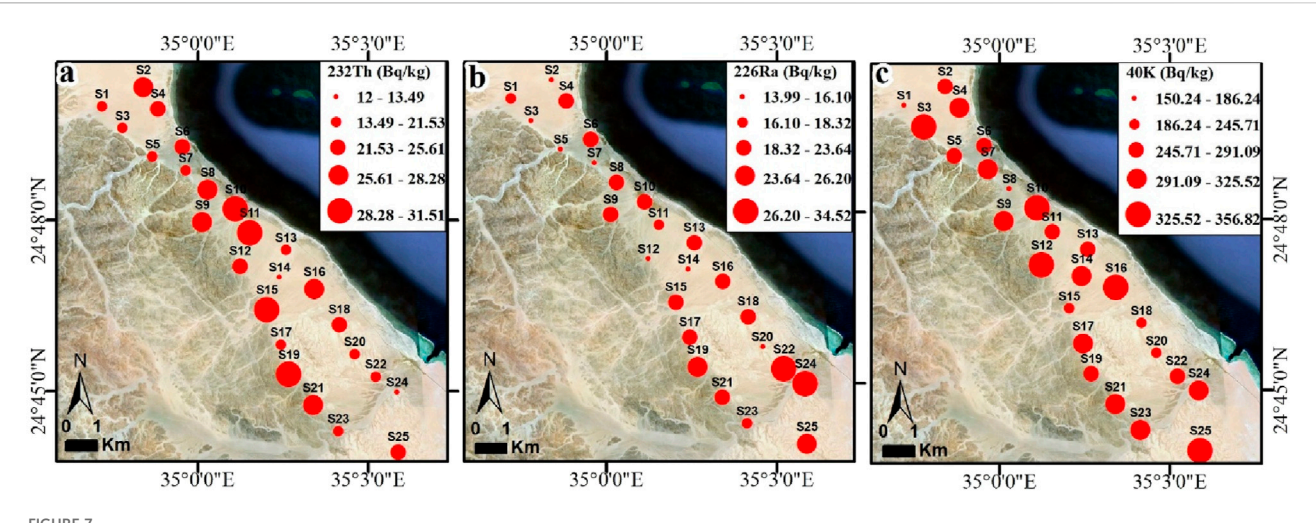


FIGURE 7
Spatial distribution of the radionuclide's concentrations (Bq/kg) of ²³²Th (a), ²²⁶Ra (b), and ⁴⁰K (c) in coastal sediments of W. Ghadir outlet, Red Sea.

remained the most concerning. Similarly, sediment quality guideline-based indices (MERMQ = 0.79, TRI = 10.04, mHQ = 1.9) indicated moderate to medium-high ecological risk, again highlighting Ni and Cr as priority contaminants. Importantly, human health risk indices showed that both non-carcinogenic (HI < 1) and carcinogenic (TCR within 10⁻⁶–10⁻⁴) risks were within acceptable limits, albeit higher than in other Red Sea sites (Saleh et al., 2025; Al-Kahtany et al., 2023). Taken together, these indices suggest that while W. Ghadir sediments are moderately to considerably enriched in certain metals—particularly Ni and Pb—their overall ecological and human health risks remain relatively low, though localized hotspots (e.g., site S5) may warrant targeted management interventions to preserve the Red Sea's coastal biodiversity and ecosystem services.

3.4 Sediment radioactivity assessment

The concentrations of radionuclides ⁴⁰K, ²²⁶Ra, and ²³²Th (Bq/Kg) were measured in 25 sediment samples collected from the W. Ghadir outlet along the Red Sea coast, with results summarized in Supplementary Table S15 and spatially illustrated in Figure 7. The average concentrations ±standard deviation were 32.07 ± 5.2 Bq/kg for ²³²Th (Figure 7a), 20.02 ± 5.24 Bq/kg for ²²⁶Ra (Figure 7b), and 289.31 ± 51.69 Bq/kg for ⁴⁰K (Figure 7c). These values are all below the global average reference levels of 45 Bq/kg for ²³²Th, 33 Bq/kg for ²²⁶Ra, and 412 Bq/kg for ⁴⁰K (Freitas and Alencar, 2004; Khaleal et al., 2023b; 2023a; UNSCEAR, 2010). The combined activity concentration of ⁴⁰K, ²²⁶Ra, and ²³²Th ranged from 188.55 to 402.97 Bq/kg, with an average of 333.39 ± 52.03 Bq/kg, which is also below the global average threshold of 420 Bq/kg (Qureshi et al., 2014; UNSCEAR, 2000).

The mean activity ratios of $^{226}\text{Ra}/^{40}\text{K}$ (ranging from 0.04 to 0.12, average: 0.08 \pm 0.02) and $^{232}\text{Th}/^{40}\text{K}$ (ranging from 0.04 to 0.15, average: 0.08 \pm 0.03) are slightly above the global average value of 0.067 (Qureshi et al., 2014). This may be attributed to the high potassium content leached from granitic source rocks. Additionally, the $^{226}\text{Ra}/^{232}\text{Th}$ ratio ranged from 0.54 to 2.89, with a mean of 0.97 \pm 0.44, slightly below the global average of 1 (Qureshi et al., 2014). The

sediment samples followed a consistent activity trend: 40 K > 232 Th > 226 Ra (Supplementary Table S15). The elevated 40 K levels are likely due to the abundance of K-bearing minerals, such as feldspars, derived from granitic rocks rich in SiO₂ (Lasheen et al., 2022; 2025; Shahrokhi et al., 2020; Zakaly et al., 2024).

Considering the current ⁴⁰K, ²²⁶Ra, and ²³²Th activity data with the figures from the prior global evaluation, which are displayed in Table 5. The level of activity that is shown is obviously below the maximum amount of (UNSCEAR, 2010), and other regions such as those of Gulf of Aqaba (Al-Trabulsy et al., 2011), Dois Rios beach, Brazil (Freitas and Alencar, 2004), Taghdoua, Saudi Arabia (Aydarous et al., 2022), Aliağa Bay, Rurkey (Özden and Aközcan, 2021), Kumaun, Himalaya, India (Ramola et al., 2011), Konya, Turkey (Özden et al., 2023), Red Sea coast (Harb, 2008), West coast. Thailand (Malain et al., 2010), Wadi El-Gemal Island, Red Sea (Khaleal et al., 2023c), Aegean coast, Greece (Shahrokhi et al., 2020), and Lake Nasser, south Egypt (Ibraheim et al., 1995) (Table 5).

A range of parameters were employed to assess radioactivity in coastal sediments collected from the Ghadir area along the Red Sea. These include absorbed dose rate (Dair), annual effective doses for outdoor and indoor exposure (AEDout and AEDin), excess lifetime cancer risk (ELCR), external and internal hazard indices (Hex and H_{in}), alpha index (I_{α}), radium equivalent activity (Ra_{eq}), and gamma index (I_v), as presented in Supplementary Table S16. The absorbed dose rate in air (Dair), which measures gamma radiation at 1 m above ground level (Kumar et al., 2024; UNSCEAR, 2000), ranged from 27.5 to 44.26 nGy/h, with an average of 36.55 \pm 4.7 nGy/h. This is below the global average of 59 nGy/h (UNSCEAR, 2010). Annual effective doses, both outdoor (AEDout) and indoor (AEDin), were calculated based on Dair using a dose conversion factor of 0.7 Sv/Gy and occupancy factors of 0.2 for outdoor and 0.8 for indoor exposure (O'Brien and Sanna, 1976; UNSCEAR, 2000). The mean AEDout ranged from 0.03 to 0.05 mSv/y, with an average of 0.04 \pm 0.01 mSv/ y, well within the UNSCEAR (2010) recommended limit of 0.07 mSv/y. Similarly, AEDin ranged from 0.13 to 0.22 mSv/y, averaging 0.18 ± 0.02 mSv/y, which also remains below the recommended threshold (Abdul Sani et al., 2022; Al-Mur et al., 2025; Zakaly et al., 2024).

TABLE 5 Comparison of ²²⁶Ra, ²³²Th, and ⁴⁰K levels of W. Ghadir area with different areas in Egypt and worldwide.

Location	²²⁶ Ra (Bq/kg)	⁴⁰ K (Bq/kg)	²²⁶ Th (Bq/kg)	References
Aqaba Gulf	5.18-29.25	324.55-1,133.04	5.28-58.87	Al-Trabulsy et al. (2011)
Dois Rios beach, Brazil	39	412	48	Freitas and Alencar (2004)
Aliağa Bay, İzmir, Turkey	45.94	721.27	50.23	Özden and Aközcan (2021)
Lake Nasser, Egypt	21	155	23	Ibraheim et al. (1995)
Red Sea coast, Egypt	5–51	159–1761	4–33	Harb (2008)
Nile Delta and Middle Egypt	18	316	17	Ibrahiem et al. (1993)
Kumaun Himalaya, India	66.7	887.1	79.4	Ramola et al. (2011)
Konya, Turkey	28.24	366.03	29.7	Özden et al. (2023)
Wadi El-Gemal Island, Egypt	12.49	325.13	12.63	Khaleal et al. (2023c)
West coast, Thailand	2.7-23.5	10.7-654.3	3.0-31.2	Malain et al. (2010)
Saudi Arabia	6-54	299-761	7–52	Aydarous et al. (2022)
Highlands of northern Jordan	42.5	291.1	26.7	Al-Hamarneh and Awadallah (2009)
Aegean coast, Greece	9–31	426-740	9–67	Shahrokhi et al. (2020)
W. Ghadir outlet, Egypt	21.02	289.31	23.07	Present work

The excess lifetime cancer risk (ELCR) values for the coastal sediment samples showed a mean of $0.16 \pm 0.02 \times 10^{-3}$, ranging from 0.12×10^{-3} to 0.19×10^{-3} , all within the acceptable limit of 0.29×10^{-3} (Fathy et al., 2023; Lasheen et al., 2022; Qureshi et al., 2014). These results suggest that long-term exposure to the studied shoreline sediments does not pose a significant cancer risk. For a comparison, Büyükuslu et al. (2018) measured the radionuclide concentrations at Giresun University, Turkey using standard dose assessment models. The results showed that all values, including effective doses and ELCR, remained below international guideline limits, providing a baseline for future monitoring. The internal (H_{in}) and external (Hex) hazard indices, which evaluate the potential health risks from radiation exposure (UNSCEAR, 2010; Lasheen et al., 2022; Abbasi et al., 2020), also indicated no significant risk. Hex values ranged from 0.16 to 0.25, with a mean of 0.21 \pm 0.03 Bq/kg, while $H_{\rm in}$ values ranged from 0.19 to 0.32, averaging 0.26 ± 0.04 Bq/kg—both well below the safety threshold of 1 (Abbasi et al., 2020; Attallah et al., 2018; European Commission, 1999; Özden et al., 2023). The alpha index (I_a), used to assess the potential hazard from alpha-emitting radionuclides, also remained low, with values ranging from 0.07 to 0.17 and a mean of 0.11 \pm 0.03 Bq/kg, further confirming the minimal health risk associated with the samples (Lasheen et al., 2025).

Radium equivalent activity (Ra_{eq}), which accounts for contributions from alpha and gamma radiation, ranged from 58.11 to 92.15 Bq/kg, with a mean of 76.28 \pm 10.04 Bq/kg, well below the recommended maximum of 370 Bq/kg (UNSCEAR, 2010). Finally, the gamma index (I $_{\gamma}$), used to evaluate external gamma exposure, had values between 0.21 and 0.34, with an average of 0.28 \pm 0.04 Bq/kg, also below the permissible limit of 1, indicating that the sediments pose no radiological threat to human health.

Supplementary Figure S2 presents a list of key minerals identified using Environmental Scanning Electron Microscopy (ESEM), selected with the aid of a binocular microscope and subsequently classified. The primary heavy minerals separated

include zircon, cassiterite, magnetite, ilmenite, pyrite, and garnet. Garnet is widely used in the production of abrasive powders, grinding materials, and as a processing medium in water jet cutting. It can also be partially used as a fine aggregate replacement in mortar, influencing both the mechanical strength and water absorption capacity of the final mix (Ruslan et al., 2024). According to ESEM analysis, the garnet particles examined are predominantly composed of almandine and spessartine, with elemental compositions of Fe (23.9%), Mn (8.8%), Al (11.4%), Mg (1.4%), and Ca (1%) (Supplementary Figure S2a).

Ilmenite (FeTiO₃), the most abundant titanium-bearing mineral in placer deposits and coastal zones, is a key source for producing metallic titanium. Titanium, known for its high strength-to-density ratio, is used in abrasive tools, cutting wheel tips, and various industrial applications (Padmanabhan et al., 1990; Saleh et al., 2024). ESEM analysis of the studied ilmenite grains revealed the following elemental composition: Fe (34.6%), Ti (19.8%), Mg (1.7%), Mn (1.9%), and Ca (0.6%) (Supplementary Figure S2b). Magnetite (Fe₃O₄) is a common iron oxide mineral found in sedimentary, metamorphic, and igneous rocks, often occurring alongside hematite. It is one of the most widely mined sources of iron ore. ESEM analysis of the magnetite grains in this study revealed a composition dominated by Fe (46.5%), with notable amounts of Ti (8%), Cr (5.1%), Mg (4.3%), and Al (3.2%) (Supplementary Figure S2c).

Pyrite (FeS₂) is the most abundant sulfide mineral in hydrothermal environments and remains stable at temperatures up to 740 °C. This thermal stability explains the observed decline in gold (Au) concentrations beyond this threshold, supporting the established understanding that Au coexists with arsenic (As) in pyrite only when As levels are below 13 wt% (Börner et al., 2021; Kutzschbach et al., 2024). ESEM measurements of pyrite grains in the samples show major components of S (48.9%), Fe (43.3%), and Al (2.2%) (Supplementary Figure S2d). Cassiterite, the primary ore

of tin (Sn), occurs in various geological settings, including granites and pegmatites (Liu et al., 2023). It typically forms as euhedral to subhedral crystals and varies in color from black to reddish-brown. In the analyzed stream sediments, cassiterite is characterized by a high Sn content (62.2%) and minor amounts of Fe (0.6%), Mg (1%), and Ca (2.97%) (Supplementary Figure S2e).

Zircon is a widely distributed and relatively common mineral in the Earth's crust, found in most sedimentary and igneous rocks, especially granites (Fathy et al., 2023; Lasheen et al., 2022; Saleh et al., 2024). Due to its exceptionally high melting point and durability, zircon is used in the steel industry as an abrasive and for furnace linings. In the studied stream sediments, zircon is the most abundant non-opaque mineral. ESEM analysis of euhedral zircon grains revealed major elements including Zr (40.3%), Ti (2.5%), Hf (1.3%), and Fe (0.8%) (Supplementary Figure S2f).

4 Conclusion

The sediments of W. Ghadir outlet show localized enrichment and contamination primarily from Ni and Pb, which posed the highest ecological and toxic risks, while overall non-carcinogenic (HI < 1) and carcinogenic (TCR within safe limits) risks to humans were minimal. Radiological assessments of ²³²Th, ²²⁶Ra, and ⁴⁰K indicated activity concentrations below global reference limits, with all radiological indices within safe thresholds, suggesting negligible radiation hazards. These findings highlight the need for targeted coastal management strategies to mitigate Ni and Pb inputs, particularly from mining and tourism activities, while preserving ecological integrity. Regular monitoring of sediment quality, combined with pollution control measures, is recommended to safeguard marine ecosystems and human health.

Data availability statement

The original contributions presented in the study are included in the article/Supplementary Material, further inquiries can be directed to the corresponding authors.

Author contributions

GS: Methodology, Conceptualization, Formal Analysis, Investigation, Writing – review and editing. HS: Resources, Funding acquisition, Writing – review and editing, Supervision. EL: Data curation, Conceptualization, Visualization, Supervision, Writing – original draft, Investigation, Writing – review and editing.

References

Abbasi, A., Zakaly, H. M. H., and Mirekhtiary, F. (2020). Baseline levels of natural radionuclides concentration in sediments East coastline of North Cyprus. *Mar. Pollut. Bull.* 161, 111793. doi:10.1016/I.MARPOLBUL.2020.111793

Abdelaal, A., Sultan, M., Elhebiry, M., Krishnamurthy, R. V., and Sturchio, N. (2021). Integrated studies to identify site-specific parameters for environmentally benign mining operations: a case study from the Sukari Gold Mine, Egypt. Sci. Total Environ. 750, 141654. doi:10.1016/j.scitotenv.2020.141654

MK: Investigation, Writing – review and editing, Methodology, Formal Analysis. AE: Supervision, Funding acquisition, Writing – review and editing, Methodology. MS: Supervision, Funding acquisition, Data curation, Writing – review and editing. IS: Supervision, Validation, Writing – review and editing, Funding acquisition. AA: Writing – review and editing, Writing – original draft, Software, Data curation.

Funding

This work was supported and funded by the Deanship of Scientific Research at Imam Mohammad Ibn Saud Islamic University (IMSIU) (grant number IMSIU-DDRSP2502).

Conflict of interest

The authors declare that the research was conducted in the absence of any commercial or financial relationships that could be construed as a potential conflict of interest.

Generative AI statement

The author(s) declare that no Generative AI was used in the creation of this manuscript.

Any alternative text (alt text) provided alongside figures in this article has been generated by Frontiers with the support of artificial intelligence and reasonable efforts have been made to ensure accuracy, including review by the authors wherever possible. If you identify any issues, please contact us.

Publisher's note

All claims expressed in this article are solely those of the authors and do not necessarily represent those of their affiliated organizations, or those of the publisher, the editors and the reviewers. Any product that may be evaluated in this article, or claim that may be made by its manufacturer, is not guaranteed or endorsed by the publisher.

Supplementary material

The Supplementary Material for this article can be found online at: https://www.frontiersin.org/articles/10.3389/fenvs.2025.1667069/full#supplementary-material

Abdelaal, A., Abdelkader, A. I., Alshehri, F., Elatiar, A., and Almadani, S. A. (2022). Assessment and spatiotemporal variability of heavy metals pollution in water and sediments of a coastal landscape at the Nile Delta. *Water (Switzerl.)* 14, 3981. doi:10. 3390/w14233981

Abdelaal, A., Lasheen, E. S. R., Mansour, A. M., Mohamed, A. W., Osman, M. R., Khaleal, F. M., et al. (2024). Assessing the ecological and health risks associated with heavy metal pollution levels in sediments of Big Giftun and Abu Minqar Islands, East

Hurghada, Red Sea, Egypt. *Mar. Pollut. Bull.* 198, 115930. doi:10.1016/J.MARPOLBUL. 2023.115930

Abdul Sani, S. F., Muhamad Azim, M. K., Marzuki, A. A., Khandaker, M. U., Almugren, K. S., Daar, E., et al. (2022). Radioactivity and elemental concentrations of natural and commercial salt. *Radiat. Phys. Chem.* 190, 109790. doi:10.1016/j. radphyschem.2021.109790

Al-Hamarneh, I. F., and Awadallah, M. I. (2009). Soil radioactivity levels and radiation hazard assessment in the highlands of northern Jordan. *Radiat. Meas.* 44, 102–110. doi:10.1016/J.RADMEAS.2008.11.005

Al-Kahtany, K., and El-Sorogy, A. S. (2023). Contamination and health risk assessment of surface sediments along Ras Abu Ali Island, Saudi Arabia. *J. King Saud. Univ. Sci.* 35, 102509. doi:10.1016/j.jksus.2022.102509

Al-Kahtany, K., Nour, H. E., El-Sorogy, A. S., and Alharbi, T. (2023). Ecological and health risk assessment of heavy metals contamination in mangrove sediments, Red Sea coast. *Mar. Pollut. Bull.* 192, 115000. doi:10.1016/j.marpolbul.2023.115000

Al-Mur, B. A., and Gad, A. (2022). Radiation hazard from natural radioactivity in the marine sediment of Jeddah Coast, Red Sea, Saudi Arabia. *J. Mar. Sci. Eng.* 10, 1145. doi:10.3390/imse10081145

Al-Mur, B. A., Aljahdali, M. H., Almeelbi, T., and Lasheen, E. S. R. (2025). Spatial radionuclide distribution, mineralogy, and radiological evaluation of the Jeddah shoreline sediments, Red Sea, Saudi Arabia. *Environ. Monit. Assess.* 197, 593. doi:10. 1007/s10661-025-13986-8

Al-Trabulsy, H. A., Khater, A. E. M., and Habbani, F. I. (2011). Radioactivity levels and radiological hazard indices at the Saudi coastline of the Gulf of Aqaba. *Radiat. Phys. Chem.* 80, 343–348. doi:10.1016/j.radphyschem.2010.09.002

AlZahrani, J. H., Alharbi, W. R., and Abbady, A. G. E. (2011). Radiological impacts of natural radioactivity and heat generation by radioactive decay of phosphorite deposits from northwestern Saudi Arabia. *Aust. J. Basic Appl. Sci.* 5.

Ardila, P. A. R., Alonso, R. Á., Valsero, J. J. D., García, R. M., Cabrera, F. Á., Cosío, E. L., et al. (2023). Assessment of heavy metal pollution in marine sediments from southwest of Mallorca Island, Spain. *Environ. Sci. Pollut. Res.* 30, 16852–16866. doi:10.1007/s11356-022-25014-0

Attallah, M. F., Hilal, M. A., and Mohamed, Y. T. (2018). Preliminary investigations on reducing the high radiation risk level of TENORM scale waste from petroleum industry. *Radiochim. Acta* 106, 793–800. doi:10.1515/ract-2017-2904

Aydarous, A., Zeghib, S., Abdullahi, S., and Al-Subaie, H. (2022). Radiological hazard assessment and sensitivity analysis for soil samples in Taghdoua area of Ranyah, Saudi Arabia. *J. Radiat. Res. Appl. Sci.* 15, 119–128. doi:10.1016/J.JRRAS.2022.05.006

Badawy, W. M., El-Taher, A., Frontasyeva, M. V., Madkour, H. A., and Khater, A. E. M. (2018). Assessment of anthropogenic and geogenic impacts on marine sediments along the coastal areas of Egyptian Red Sea. *Appl. Radiat. Isotopes* 140, 314–326. doi:10.1016/j.apradiso.2018.07.034

Benson, N. U., Adedapo, A. E., Fred-Ahmadu, O. H., Williams, A. B., Udosen, E. D., Ayejuyo, O. O., et al. (2018). A new method for assessment of sediment-associated contamination risks using multivariate statistical approach. *MethodsX* 5, 268–276. doi:10.1016/j.mex.2018.03.005

Büyükuslu, H., Özdemir, F. B., Öge, T. Ö., and Gökce, H. (2018). Indoor and tap water radon (222Rn) concentration measurements at Giresun University Campus areas. *Appl. Radiat. Isotopes* 139, 285–291. doi:10.1016/j.apradiso.2018.05.027

Börner, F., Keith, M., Smith, D. J., Barry, T. L., Neumann, T., and Klemd, R. (2021). Fingerprinting fluid evolution by trace elements in epithermal pyrite, Vatukoula Au-Te deposit, Fiji. *Ore Geol. Rev.* 137, 104314. doi:10.1016/j.oregeorev.2021.104314

CSQG (2007). Canadian Soil Quality Guidelines (CSQG) for the protection of environmental and human health: summary tables. Winnipeg, MB, Canada. Canadian Council of Ministers of the Environment CCME. doi:10.1177/004947559702700223

Dean, W. E. (1974). Determination of Carbonate and organic matter in calcareous sediments and sedimentary rocks by loss on ignition: comparison with other methods. SEPM J. Sediment. Res. 44. doi:10.1306/74d729d2-2b21-11d7-8648000102c1865d

El-Sorogy, A. S., Youssef, M., Al-Kahtany, K., and Saleh, M. M. (2020). Distribution, source, contamination, and ecological risk status of heavy metals in the Red Sea-Gulf of Aqaba coastal sediments, Saudi Arabia. *Mar. Pollut. Bull.* 158, 111411. doi:10.1016/j. marpolbul.2020.111411

Emenike, P. G. C., Tenebe, I. T., Neris, J. B., Omole, D. O., Afolayan, O., Okeke, C. U., et al. (2020). An integrated assessment of land-use change impact, seasonal variation of pollution indices and human health risk of selected toxic elements in sediments of River Atuwara, Nigeria. *Environ. Pollut.* 265, 114795. doi:10.1016/j.envpol.2020.114795

Ercegovac, M., and Kostić, A. (2006). Organic facies and palynofacies: nomenclature, classification and applicability for petroleum source rock evaluation. *Int. J. Coal Geol.* 68, 70–78. doi:10.1016/J.COAL.2005.11.009

European Commission (1999). Radiation Protection 112: radiological protection principles concerning the natural radioactivity of building materials. Luxembourg: Office for Official Publications of the European Communities.

Fang, T. H., and Chang, J. R. (2023). The geochemical and environmental characteristics of trace metals in coastal sediment discharge off the Mailiao

Industrial Zone of central Western Taiwan. Water (Switzerl.) 15, 250. doi:10.3390/w15020250

Farhat, H. I., Gad, A., Saleh, A., and Abd El Bakey, S. M. (2022). Risks assessment of potentially toxic elements' contamination in the Egyptian Red Sea surficial sediments. *Land (Basel)* 11, 1560–21. doi:10.3390/land11091560

Fathy, D., Zakaly, H. M. H., Lasheen, E. S. R., Elsaman, R., Alarifi, S. S., Sami, M., et al. (2023). Assessing geochemical and natural radioactivity impacts of Hamadat phosphatic mine through radiological indices. *PLoS One* 18, e0287422. doi:10.1371/JOURNAL.PONE.0287422

Folk, R. L. (1980). Petrology of sedimentary rocks. Austin: Hemphill Publishing Company, 190.

Freitas, A. C., and Alencar, A. S. (2004). Gamma dose rates and distribution of natural radionuclides in sand beaches—Ilha Grande, Southeastern Brazil. *J. Environ. Radioact.* 75, 211–223. doi:10.1016/J.JENVRAD.2004.01.002

Gopal, V., Krishnamurthy, R. R., Vignesh, R., Sabari Nathan, C., Anshu, R., Kalaivanan, R., et al. (2023). Assessment of heavy metal contamination in the surface sediments of the Vedaranyam coast, Southern India. *Reg. Stud. Mar. Sci.* 65, 103081. doi:10.1016/j.rsma.2023.103081

Hakanson, L. (1980). An ecological risk index for aquatic pollution control.a sedimentological approach. *Water Res.* 14, 975–1001. doi:10.1016/0043-1354(80) 90143-8

Haluschak, P. (2006). Laboratory methods of soil analysis. Canada-Manitoba soil Surv.

Harb, S. (2008). Natural radioactivity and external gamma radiation exposure at the coastal Red Sea in Egypt. *Radiat. Prot. Dosim.* 130, 376–384. doi:10.1093/RPD/NCN064

Ibraheim, M. N., Shawky, S., and Amer, H. A. (1995). Radioactivity levels in Lake Nasser sediments. *Appl. Radiat. Isotopes* 46, 297–299. doi:10.1016/0969-8043(94) 00144-O

Ibrahiem, N. M., Abd El Ghani, A. H., Shawky, S. M., Ashraf, E. M., and Farouk, M. A. (1993). Measurement of radioactivity levels in soil in the Nile Delta and Middle Egypt. Health Phys. 64, 620–627. doi:10.1097/00004032-199306000-00007

Jalali, M., Moradi, F., Jalali, M., and Wang, J. (2023). Risk assessment of available and total heavy metals contents in various land use in calcareous soils. *Environ. Earth Sci.* 82, 298–19. doi:10.1007/s12665-023-10949-5

Kabata-Pendias, A., and Mukherjee, A. B. (2007). Trace elements from soil to human. Berlin: Springer, 550. doi:10.1007/978-3-540-32714-1

Kamar, M. S., Moghazy, N. M., and Saleh, G. M. (2021). Pan-African rare metals bearing pegmatites in Wadi Ghadir, South Eastern desert, Egypt: the geochemical evolution and implications for mineralization. SN Appl. Sci. 3, 427–23. doi:10.1007/s42452-021-04414-w

Khaleal, F. M., El-Bialy, M. Z., Saleh, G. M., Abdelaal, A., Kamar, M. S., Omar, M. M., et al. (2023a). Environmental risk assessment of naturally radioactive beryl-bearing rocks, Sinai and Eastern Desert, Egypt. *J. Radioanal. Nucl. Chem.* 332, 3991–4008. doi:10.1007/s10967-023-09092-z

Khaleal, F. M., El-Bialy, M. Z., Saleh, G. M., Lasheen, E. S. R., Kamar, M. S., Omar, M. M., et al. (2023b). Assessing environmental and radiological impacts and lithological mapping of beryl-bearing rocks in Egypt using high-resolution sentinel-2 remote sensing images. *Sci. Rep.* 13 (1 13), 11497–20. doi:10.1038/s41598-023-38298-0

Khaleal, F. M., Tahoon, M. A., Saleh, G. M., Kamar, M. S., Zakaly, H. M. H., Zidan, I. H., et al. (2023c). Dolphin-shaped island: exploring the natural resources and radiological hazards of Wadi El Gemal Island. *Mar. Pollut. Bull.* 194, 115367. doi:10.1016/j.marpolbul.2023.115367

Kumar, N., Khyalia, B., Yadav, J., Singh, B., Gupta, V., Singh, P. P., et al. (2024). Assessment of natural radioactivity in soil around Khetri copper belt of Rajasthan, India. *J. Radioanalytical Nucl. Chem.* 333, 3185–3194. doi:10.1007/s10967-023-09301-9

Kutzschbach, M., Dunkel, F., Kusebauch, C., Schiperski, F., Börner, F., Drake, H., et al. (2024). Arsenic-poor fluids promote strong As partitioning into pyrite. *Geochim. Cosmochim. Acta.* 376, 37–53. doi:10.1016/j.gca.2024.05.027

Lasheen, E. S. R., Azer, M. K., Ene, A., Abdelwahab, W., Zakaly, H. M. H., Awad, H. A., et al. (2022). Radiological hazards and natural radionuclide distribution in granitic rocks of Homrit Waggat Area, central Eastern desert, Egypt. *Materials* 15, 4069. doi:10. 3390/MA15124069

Lasheen, E. S. R., Mansour, A. M., Mohamed, A. W., Osman, M. R., Khaleal, F. M., Tahoon, M. A., et al. (2024). Assessing the heavy metals in surface sediments of Wadi El-Gemal Island, Red Sea, Egypt: pollution levels, sources, and associated risks. *Water Air Soil Pollut.* 235, 461–22. doi:10.1007/s11270-024-07273-4

Lasheen, E. S. R., El-Badry, B. A., Mohamed, W. H., Khouqeer, G. A., Sanislav, I. V., and Sami, M. (2025). Radioactivity and aeromagnetic of magmatic suites, Arabian Nubian Shield: petrological and health risk characteristics. *J. Radiat. Res. Appl. Sci.* 18, 101910. doi:10.1016/j.jrras.2025.101910

Liu, Y., Zhang, L., Santosh, M., Dong, G., Que, C., Yang, C., et al. (2023). Emplacement and evolution of zoned plutons: Multiproxy isotopic and geochemical evidence from the peraluminous Laojunshan leucogranite suite, southwestern China, and implications on the regional geodynamic and metallogenic history. *Gondwana. Res.* 116, 89–103. doi:10.1016/j.gr.2022.12.007

- Long, E. R., and MacDonald, D. D. (1998). Human and ecological risk assessment: recommended uses of empirically derived, sediment quality guidelines for marine and estuarine ecosystems PERSPECTIVE: recommended uses of empirically derived, sediment quality Guidelines for marine and. *Hum. Ecol. Risk Assess.* 4, 1019–1039. doi:10.1080/10807039891284956
- Long, E. R., Macdonald, D. D., Smith, S. L., and Calder, F. D. (1995). Incidence of adverse biological effects within ranges of chemical concentrations in marine and estuarine sediments. *Environ. Manage* 19, 81–97. doi:10.1007/BF02472006
- Long, E. R., MacDonald, D. D., Severn, C. G., and Hong, C. B. (2000). Classifying probabilities of acute toxicity in marine sediments with empirically derived sediment quality guidelines. *Environ. Toxicol. Chem.* 19, 2598–2601. doi:10.1002/etc.5620191028
- Macdonald, D. D., Carr, R. S., Calder, F. D., Long, E. R., and Ingersoll, C. G. (1996). Development and evaluation of sediment quality guidelines for Florida coastal waters. *Ecotoxicology* 5, 253–278. doi:10.1007/BF00118995
- MacDonald, D. D., Ingersoll, C. G., and Berger, T. A. (2000). Development and evaluation of consensus-based sediment quality guidelines for freshwater ecosystems. *Arch. Environ. Contam. Toxicol.* 39, 20–31. doi:10.1007/s002440010075
- Mahmoud, M. G., El-Khir, E. A., Ebeid, M. H., Mohamed, L. A., Fahmy, M. A., Shaban, K. S., et al. (2020). An Assessment on the Coastal Seawater Quality of the Gulf of Suez, Egypt. *J. Environ. Prot.* 11, 34–47. doi:10.4236/jep.2020.111004
- Malain, D., Regan, P. H., Bradley, D. A., Matthews, M., Santawamaitre, T., and Al-Sulaiti, H. A. (2010). Measurements of NORM in beach sand samples along the Andaman coast of Thailand after the 2004 tsunami. *Nucl. Instrum. Methods Phys. Res. A* 619, 441–445. doi:10.1016/J.NIMA.2009.11.047
- Mansour, A. M. (2003). Mining, quarrying, geology and minerals at wadi El gemalhamata protected areas. Egyptian environmental policy program, MOBIS task order No. 263-M-00-03-00002-00. U.S. Agency for International Development. Available online at: https://www.abughosoun.org/wp-content/uploads/2019/04/6-Mining-Quarrying-Geology-_-Minerals-at-WGNP.pdf. (Accessed October 5, 2025).
- Miletić, A., Lučić, M., and Onjia, A. (2023). Exposure factors in health risk assessment of heavy Metal(loid)s in soil and sediment. *Met. (Basel)* 13, 1266. doi:10.3390/met13071266
- Mohammadi, A. A., Zarei, A., Majidi, S., Ghaderpoury, A., Hashempour, Y., Saghi, M. H., et al. (2019). Carcinogenic and non-carcinogenic health risk assessment of heavy metals in drinking water of Khorramabad, Iran. *MethodsX* 6, 1642–1651. doi:10.1016/j. mex.2019.07.017
- Mohammed, A. H., Khalifa, A. M., Mohamed, H. M., Abd El-Wahid, K. H., and Hanafy, M. H. (2024). Assessment of heavy metals at mangrove ecosystem, applying multiple approaches using *in-situ* and remote sensing techniques, Red Sea, Egypt. *Environ. Sci. Pollut. Res.* 31, 8118–8133. doi:10.1007/s11356-023-31625-y
- Mueller, G. (1981). Die Schwermetallbelastung der sedimente des Neckars und seiner Nebenflusse: eine Bestandsaufnahme. *Chem. ZTG* 105, 157–164.
- Nour, H. E., Alshehri, F., Sahour, H., El-Sorogy, A. S., and Tawfik, M. (2022). Assessment of heavy metal contamination and health risk in the coastal sediments of Suez Bay, Gulf of Suez, Egypt. *J. Afr. Earth Sci.* 195, 104663. doi:10.1016/j.jafrearsci. 2021.104663
- OEHHA (2023). California Office of the Environmental Health Hazard Assessment (OEHHA), U.S. toxicity criteria on chemicals evaluated by OEHHA [WWW Document]. Available online at: https://oehha.ca.gov/chemicals (Accessed January 10, 24).
- Oregioni, B., and Astone, S. (1984). The determination of selected trace metals in marine sediments by flameless/flame-atomic absorption spectrophotometry. IAEA Monaco Laboratory, Internal Report.
- Özden, S., and Aközcan, S. (2021). Natural radioactivity measurements and evaluation of radiological hazards in sediment of Aliağa Bay, İzmir (Turkey). *Arabian J. Geosciences* 14, 1–14. doi:10.1007/S12517-020-06446-9/FIGURES/11
- Özden, S., Pehlivanoğlu, S. A., and Günay, O. (2023). Evaluation of natural radioactivity in soils of Konya (Turkey) and estimation of radiological health hazards. *Environ. Monit. Assess.* 195, 1–13. doi:10.1007/S10661-023-12162-0/METRICS
- O'brien, R., and Sanna, R. (1976). The distribution of absorbed dose-rates in humans from exposure to environmental gamma rays. *Health Phys.* 30, 71–78. doi:10.1097/00004032-197601000-00007
- Padmanabhan, N. P. H., Sreenivas, T., and Rao, N. K. (1990). Processing of Ores of Titanium, Zirconium, Hafnium, Niobium, Tantalum, Molybdenum, Rhenium, and Tungsten: International Trends and the Indian Scene. *High Temp. Mater. Process.* 9, 217–248. doi:10.1515/HTMP.1990.9.2-4.217
- Qureshi, A. A., Tariq, S., Din, K. U., Manzoor, S., Calligaris, C., and Waheed, A. (2014). Evaluation of excessive lifetime cancer risk due to natural radioactivity in the rivers sediments of Northern Pakistan. *J. Radiat. Res. Appl. Sci.* 7, 438–447. doi:10.1016/J.IRRAS.2014.07.008
- RAIS (2017). Risk assessment information system in the risk exposure models for chemicals user's guide. Available online at: https://rais.ornl.gov/tools/rais_chemical_risk_guide.html.
- Ramola, R. C., Choubey, V. M., Prasad, G., Gusain, G. S., Tosheva, Z., and Kies, A. (2011). Radionuclide analysis in the soil of Kumaun Himalaya, India, using gamma ray spectrometry. *Curr. Sci.* 100.

- Ravisankar, R., Chandramohan, J., Chandrasekaran, A., Prince Prakash Jebakumar, J., Vijayalakshmi, I., Vijayagopal, P., et al. (2015). Assessments of radioactivity concentration of natural radionuclides and radiological hazard indices in sediment samples from the East coast of Tamilnadu, India with statistical approach. *Mar. Pollut. Bull.* 97, 419–430. doi:10.1016/J.MARPOLBUL.2015.05.058
- Reimann, C., Filzmoser, P., Garrett, R. G., and Dutter, R. (2008). Statistical data analysis explained: applied environmental statistics with R. Statistical data analysis explained. *Appl. Environ. Statistics R*, 1–343. doi:10.1002/9780470987605
- Ruslan, H. N., Muthusamy, K., Muzafar Shah, M. H., Mat Yahaya, F., and Zulkarnain, F. (2024). Properties of concrete containing spent garnet as fine aggregate replacement. *IOP Conf. Ser. Earth Environ. Sci.* 1369, 012039. doi:10.1088/1755-1315/1369/1/012039
- Saleh, G. M., Lasheen, E. S. R., Foi, M., Abdalla, F., and Abdelaal, A. (2025). Assessment of radioactivity and heavy metal pollution levels in the coastal sediments in the Red Sea Region of Sharm El Luli, Egypt. *Water, Air, Soil Pollut.* 236 (5 236), 319–324. doi:10.1007/S11270-025-07962-8
- Saleh, G. M., Kamh, S. Z., Abdalla, F., Kilias, A., and Lasheen, E. S. R. (2024). A new occurrence of rift-related damtjernite (ultramafic) lamprophyre, Gebel Anweiyib area, Arabian Nubian shield: Insights from bulk rock geochemistry and remote sensing data analysis. *Phys. Chem. Earth Parts ABC*133, 103530. doi:10. 1016/j.pcc.2023.103530
- Saralioglu, E., and Vatandaslar, C. (2022). Land use/land cover classification with Landsat-8 and Landsat-9 satellite images: a comparative analysis between forest- and agriculture-dominated landscapes using different machine learning methods. *Acta Geod. Geophys.* 57, 695–716. doi:10.1007/s40328-022-00400-9
- Shahrokhi, A., Adelikhah, M., Chalupnik, S., Kocsis, E., Toth-Bodrogi, E., and Kovács, T. (2020). Radioactivity of building materials in Mahallat, Iran an area exposed to a high level of natural background radiation attenuation of external radiation doses. *Mater. Construcción* 70, e233. doi:10.3989/MC.2020.03820
- Song, X., Dong, J., Wang, H., Xie, H., Yu, Y., Geng, L., et al. (2023). Factors influencing the distribution of organic carbon in four different coastal sedimentary environments. *J. Soils Sediments* 23, 1539–1551. doi:10.1007/s11368-022-03423-5
- Tomlinson, D. L., Wilson, J. G., Harris, C. R., and Jeffrey, D. W. (1980). Problems in the assessment of heavy-metal levels in estuaries and the formation of a pollution index. *Helgoländer Meeresunters.* 33, 566–575. doi:10.1007/BF02414780
- Turekian, K. K., and Wedepohl, K. H. (1961). Distribution of the elements in some major units of the earth's crust. *Geol. Soc. Am. Bull.* 72, 175. doi:10.1130/0016-7606(1961)72[175:doteis]2.0.co;2
- UNSCEAR (2000). Sources and effects of risks ionizing radiation. Report to the general asembly, with scientific annexes. New York, NY: United Nations.
- UNSCEAR (2010). Sources and effects of ionizing radiation. New York, NY: United Nations.
- U.S. EPA (1989). Risk assessment guidance for superfund volume 1 human health evaluation manual (Part A). EPA/540/1-89/002, office of emergency and remedial response. Washington, DC: U.S. Environmental Protection Agency.
- U.S. EPA (2002). Supplemental guidance for developing soil screening levels for superfund sites. Office of solid waste and emergency response, OSWER 9355.4-24. Washington, DC: U.S. Environmental Protection Agency.
- U.S. EPA (2005). Guidelines for carcinogen risk assessment. Risk assessment forum. Washington, DC: U.S. Environmental Protection Agency. EPA/630/P-03/001F.
- U.S. EPA (2007). Framework for metals risk assessment. Office of the science advisor, risk assessment forum. Washington, DC: U.S. Environmental Protection Agency. EPA 120/R-07/001.
- Vaezi, A., and Lak, R. (2023). Sediment texture, geochemical variation, and ecological risk assessment of major elements and trace metals in the sediments of the northeast Persian Gulf. *Minerals* 13, 850. doi:10.3390/min13070850
- Wan, D., Gao, J., Song, R., Song, L., and Ning, D. (2023). Uncertainties in pollution and risk assessments of heavy metals in Lake sediments using regional background soils in China. *Toxics* 11, 613. doi:10.3390/toxics11070613
- Xu, Z., Shi, M., Yu, X., and Liu, M. (2022). Heavy metal pollution and health risk assessment of vegetable-soil systems of facilities irrigated with wastewater in Northern China. *Int. J. Environ. Res. Public Health* 19, 9835. doi:10.3390/ijerph19169835
- Yüksel, B., and Fikret, U. (2025). Pollution analysis of metals in the sediments of lagoon lakes in Türkiye: toxicological risk assessment and source insights. *Process Saf. Environ. Prot.* 193, 665–682. doi:10.1016/j.psep.2024.11.085
- Zakaly, H. M. H., Awad, H. A., Lasheen, E. S. R., Issa, S. A. M., Elsaman, R., Khandaker, M. U., et al. (2024). Radiometric and petrographic characterization of El-Yatima granite: evaluating radiological risks and mineralogical features. *Radiat. Phys. Chem.* 224, 111992. doi:10.1016/J.RADPHYSCHEM.2024.111992
- Zhang, Z., Juying, L., Mamat, Z., and QingFu, Y. (2016). Sources identification and pollution evaluation of heavy metals in the surface sediments of Bortala River, Northwest China. *Ecotoxicol. Environ. Saf.* 126, 94–101. doi:10.1016/j.ecoenv.2015.12.025
- Zhao, Z., Liu, Q., Liao, Y., Yu, P., Tang, Y., Liu, Q., et al. (2023). Ecological risk assessment of trace metals in sediments and their effect on benthic organisms from the south coast of Zhejiang province, China. *Mar. Pollut. Bull.* 187, 114529. doi:10.1016/j.marpolbul.2022.114529